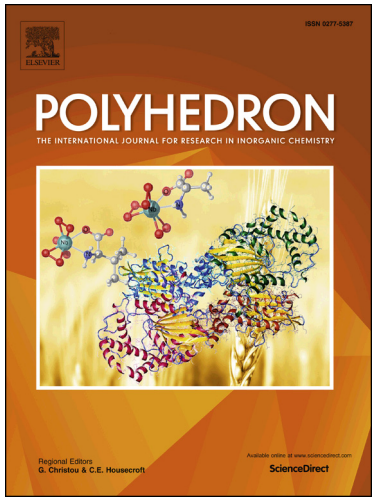

Group 10 metal complexes of dithiocarbamates derived from primary anilines: synthesis, characterization, computational and antimicrobial studies

Felicia F. Bobinihi, Damian C. Onwudiwe, Anthony C. Ekennia, Obinna C. Okpareke, Charmaine Arderne, Joseph R. Lane

PII: S0277-5387(18)30722-8
DOI: https://doi.org/10.1016/j.poly.2018.10.073
Reference: POLY 13551

To appear in: *Polyhedron*

Received Date: 14 September 2018
Accepted Date: 27 October 2018

Please cite this article as: F.F. Bobinihi, D.C. Onwudiwe, A.C. Ekennia, O.C. Okpareke, C. Arderne, J.R. Lane, Group 10 metal complexes of dithiocarbamates derived from primary anilines: synthesis, characterization, computational and antimicrobial studies, *Polyhedron* (2018), doi: https://doi.org/10.1016/j.poly.2018.10.073

Group 10 metal complexes of dithiocarbamates derived from primary anilines: synthesis, characterization, computational and antimicrobial studies

[1,2,3] Felicia F. Bobinihi, [1,2]Damian C. Onwudiwe*, [4]Anthony C. Ekennia, [5,6]Obinna C. Okpareke, [7]Charmaine Arderne, [6]Joseph R. Lane.

[1]Material Science Innovation and Modelling (MaSIM) Research Focus Area, Faculty of Natural and Agricultural Sciences, North-West University (Mafikeng Campus), Private Bag X2046, Mmabatho, South-Africa.

[2]Department of Chemistry, School of Physical and Chemical Sciences, Faculty of Natural and Agricultural Sciences, North-West University (Mafikeng Campus), Private Bag X2046, Mmabatho 2735, South Africa.

[3]Federal college of Education, P.M.B. 1026, Okene, Kogi-State, Nigeria

[4]Department of Chemistry, Alex Ekwueme Federal University Ndufu-Alike (AE-FUNAI), PMB 1010 Abakaliki, Ebonyi State, Nigeria.

[5]Department of Pure and Industrial Chemistry, University of Nigeria, Nsukka 410001, Enugu State, Nigeria.

[6] School of Science, University of Waikato, Private Bag 3105, Hamilton, New Zealand.

[7]Department of Chemistry, University of Johannesburg, PO Box 524, Auckland Park, Johannesburg 2006, South Africa.

* Corresponding author

E-mail: Damian.Onwudiwe@nwu.ac.za Tel: (+27) 18 389 2545; Fax: +27 18 389-2420

Abstract

Dithiocarbamate ligands obtained from primary amines, namely N-phenylaniline, 4-methylaniline and 4-ethylaniline, and represented as L^1, L^2 and L^3 respectively, have been used to prepare some Ni(II), Pd(II) and Pt(II) complexes. The complexes were characterized by NMR, FTIR spectroscopy and elemental analysis. The spectroscopic data showed that the ligands were chelated to the metal ions in a bidentate mode. The complexes $[Pt(L^1)_2]$, $[Pt(L^3)_2]$, and $[Pd(L^1)_2]$ were further characterized by single crystal X-ray analysis and distorted square planar geometries were confirmed in all cases. The magnetic susceptibility measurements of the nickel complexes suggest a square planar geometry for the diamagnetic compounds. Thermal decomposition studies of the complexes gave their respective metal sulfides as residues. Geometry optimization and harmonic frequency calculations of the ligands and the complexes were carried out using density functional theory (DFT). Molecular electrostatic potential energy calculations were used to support the coordination through the dithio-sulfur groups of the three dithiocarbamate ligands. Non-covalent interaction (NCI)

theory analysis was used to reveal the different intra and intermolecular interactions in the hydrogen bonded structures of the platinum and palladium complexes. Antimicrobial screening, conducted using selected microbes, showed that the complexes gave moderate to very active antimicrobial activities against Gram negative (*Escherichia coli, Klebsiella Pneumonia* and *Pseudomonas Aeruginosa*), Gram positive (*Bacillus cereus* and *Staphylococcus aureus*) and fungi (*Candida albicans* and *Aspergillus flavus*) organisms at a concentration of at 50 μg/mL. However, the $[Pt(L^3)_2]$ complex gave the best antimicrobial properties with an inhibitory zone range of 8-26 mm.

Keywords: Dithiocarbamates; Group 10 metals; Antimicrobial; DFT

Introduction

Dithiocarbamates derived from primary and secondary amines have been reported to have similar ligating properties to different metal ions. However, metal complexes of secondary amine-derived dithiocarbamates $[(R_2CNS_2)_2M]$ have been extensively studied owing to their greater stability than those of the primary amine analogues $[(RHCNS_2)_2M]$. The latter can easily be decomposed to give the corresponding isothiocyanates due to the presence of an acidic proton on the nitrogen atom of the thioureide [1, 2]. However, the stabilities of metal complexes of dithiocarbamates derived from primary amines have been reported to improve on coordination to metal ions and on storage under low temperatures [3]. The NH site on metal dithiocarbamate complexes of the form $[(RHCNS_2)_2M]$ stimulates the transfer of a proton between ligands through N-H···S hydrogen bonds [4]. They are also capable of providing hydrogen bonding for basic anion N-H deprotonation, which could serve as the signal-output of certain anion-receptor interactions [5]. The presence of the acidic proton (NH) has been reported to promote the lipophilicity of the metal complexes, thus improving permeability through cell walls of microbial strains [3], and enhancing their antimicrobial potentials compared to their *N, N* analogues of the form $[(R_2CNS_2)_2M]$.

Group 10 metal complexes of aryl or alkyl dithiocarbamates synthesized from secondary amines have been extensively reported [6]. The success of cisplatin inspired an extensive search for metal complexes of this triad with similar or better anticancer potentials. A nickel(II) bis(dithiocarbamate) complex was first reported by Delepine, while palladium(II) and platinum(II) bis(dithiocarbamate) complexes were first prepared by Malatesta [7]. Since

then, group 10 metal complexes have been explored in a number of biological areas due to their antimicrobial and anticancer properties [8-11]. They have also been reported to be good precursors for nickel sulfide, palladium sulfide and platinum sulfide nanoparticles through the thermal decomposition of their respective metal dithiocarbamate complexes [12]. However, nickel(II), palladium(II) and platinum(II) complexes of primary amine-derived aryl or alkyl dithiocarbamates are rarely studied.

Due to the peculiar characteristics of the acidic proton in the overall antimicrobial potentials of metal complexes of primary amine derived dithiocarbamates and the chemical diversity of dithiocarbamate complexes, we report herein group 10 metal complexes of dithiocarbamates derived from different *N*-substituted anilines. The effects of the different substituents on the nitrogen atom of the thioureide group on the spectral properties of the complexes are discussed and the antimicrobial potentials of the complexes were also investigated.

2.0 Experimental

2.1 Materials

Analar grade nickel(II) chloride, palladium(II) chloride, platinum(II) chloride, *N*-phenylaniline, *p*-methylaniline, *p*-ethylaniline, ammonium hydroxide and tetrahydrofuran (THF) were obtained from Sigma–Aldrich. Carbon disulfide and sodium hydroxide were purchased from Merck. All materials were used as supplied without further purification.

2.2. Physical measurements

An Elementar Vario EL Cube was used for the elemental (CHNS) analysis. Infrared spectra were recorded on a Bruker Alpha-P FTIR spectrometer in the 400–4000 cm^{-1} range. A 600 MHz Bruker Avance III NMR spectrophotometer was used for the NMR spectral analysis. TMS was used as an internal standard. Room temperature magnetic moments and molar conductance measurements were recorded on Sherwood susceptibility balance MSB Mark 1 and Hanna conductivity model H19991300 meters respectively.

2.3 Preparation of the ligands

Preparation of ammonium N-phenyldithiocarbamate (L^1)

To an equimolar mixture of ammonium hydroxide (15 mL, 0.05 mol) and *N*-phenyl aniline (4.6 mL, 0.05 mol) in an ice bath, carbon disulfide (3.0 mL, 0.05 mol) was added in small portions. After stirring for 6 h, the solidified mass was filtered under suction, rinsed with diethyl ether to give white solids, which were stored in the refrigerator.

Yield: 6.97 g, 75%; Selected FTIR, ν(cm^{-1}): 1452 (C=N), 1226 (C_2─N), 1018 (C=S), 3035 (=C-H), 2818 (-C-H), 3283 (N-H). ^{1}H NMR ($CDCl_3$) δ, ppm: 6.89-7.88 (m, 10H, C_6H_5), 10.12 (s, 2H, NH); ^{13}C NMR ($CDCl_3$) δ, ppm: 121.96-128.23 (C_6H_5), 196.1 (–CS_2).

Preparation of sodium p-methylphenyldithiocarbamate (L^2)

Sodium hydroxide (1.00 g, 0.025 mol) was dissolved in 20 mL THF and added to a 20 mL THF solution of CS_2 (1.5 mL, 0.025 mol). To this solution, *p*-methylaniline (2.70 g, 0.025 mol) was added and the solution was stirred for 6 h under an N_2 atmosphere. The resulting precipitate was filtered and re- precipitated in acetone to give a white precipitate which was dried under vacuum.

Yield: 4.0 g, 74%; Selected FTIR, ν(cm^{-1}): 1502 (C=N), 1215(C_2─N), 988 (C=S), 3031 (=C-H), 2920 (-C-H), 3326 (N-H); ^{1}H NMR ($CDCl_3$) δ, ppm: 6.96-7.81 (m, 10H, C_6H_5), 10.10 (s, 2H, NH), 2.34 (s, 6H, CH_3). ^{13}C NMR ($CDCl_3$) δ, ppm: 123.5-128.9 (C_6H_5), 21.3 (CH_3), 196.5 (–CS_2).

Preparation of sodium p-ethylphenyldithiocarbamate (L^3)

Sodium hydroxide (2.0 g, 0.05 mol) dissolved in 5 mL of water was added to carbon disulfide (3.0 mL, 0.05 mol) and the resulting solution was stirred in an ice bath. After 30 min, 4-ethyl aniline (6.2 mL, 0.05 mol) was added to the solution and stirred for 3 h. The resulting precipitate was filtered and re-precipitated in acetone to give a white precipitate, which was dried under vacuum.

Yield: 7.10 g, 65%: Selected FTIR, ν(cm^{-1}): 1507 (C=N), 1225 (C_2─N), 1014 (C=S), 3019 (=C-H), 2921 (-C-H), 3201 (N-H):
^{1}H NMR ($CDCl_3$) δ, ppm: 7.09-7.46 (m, 10H, C_6H_5), 10.10 (s, 2H, NH), 1.19 (t, 6H, CH_3),

2.58 (q, 4H, CH_2); ^{13}C NMR ($CDCl_3$) δ, ppm: 120.50-144.0 (C_6H_5), 15.73 (CH_3), 27.72 (CH_2), 179.30 (–CS_2).

Preparation of the metal dithiocarbamate complexes (ML^1-ML^3, M = Ni, Pd, Pt)

An aqueous solution of 0.625 mmol of the respective metal salts ($NiCl_2 \cdot 6H_2O$, 0.149 g; Na_2PdCl_4, 0.184 g; K_2PtCl_4, 0.259 g) was added to a stirring 25 mL aqueous solution of 1.250 mmol of the different ligands, L^1 (0.233 g), L^2 (0.256 g) and L^3 (0.274 g). The reaction mixture was stirred for 1 h and the different resulting colored precipitates were filtered off, washed with cold ethanol and dried in a vacuum.

(1) [Ni(L^1)$_2$]. Yield: 1.10 g, 81%; M.Pt.: 205-207 °C; Selected FTIR, ν(cm^{-1}): 1468 (C=N), 1292 (C_2─N), 958 (C=S), 3166 (=CH−H), 2953 (H_2C−H), 3356 (NH), 411 (Ni-S); ^1H NMR ($CDCl_3$) δ, ppm: 7.2-7.4 (m, 10H, C_6H_5), 8.56 (s, 2H, NH); ^{13}C NMR ($CDCl_3$) δ, ppm: 129-137 (C_6H_5), 196.7 (–CS_2); Anal. calc for $C_{14}H_{12}N_2S_4Ni$ (395.21): C, 42.55; H, 3.06; N, 7.08; S, 32.22. Found: C, 42.05 H, 3.46; N, 7.50; S, 32.62%; μeff (BM): 0.12.

(2) [Pd(L^1)$_2$]. Yield: 0.75g, 55%; M.Pt.: 210-212 °C; Selected FTIR, ν(cm^{-1}): 1475 (C=N), 1298 (C_2─N), 965 (C=S), 3226 (=CH−H), 2999 (H_2C−H), 3365 (NH), 408 (Pd–S); ^1H NMR (CDCl3) δ, ppm: 7.3-7.6 (m, 10H, C_6H_5), 9.79 (s, 2H, NH); ^{13}C NMR ($CDCl_3$) δ, ppm: 134-145 (C_6H_5), 196.7 (CS_2); Anal. calc for $C_{14}H_{12}N_2S_4Pd$ (442.94): C, 37.96; H, 2.73; N, 6.33; S, 28.95. Found: C, 37.45; H, 2.34; N, 6.86; S, 28.40%; μeff (BM): 0.25.

(3) [Pt(L^1)$_2$]. Yield: 0.65 g, 70%; M.Pt.: 240-243 °C; Selected FTIR, ν(cm^{-1}): 1494 (C=N), 1312 (C_2─N), 977 (C=S) 3154 (=CH−H), 3001, 3375(NH); ^1H NMR ($CDCl_3$) δ, ppm: 7.3-7.9 (m, 10H, C_6H_5), 9.25 (s, 2H, NH). ^{13}C NMR ($CDCl_3$) δ, ppm: 135-145 (C_6H_5), 196.9 (–CS_2), 424 (Pt–S); Anal. calc. for $C_{14}H_{12}N_2S_4Pt$ (531.60): C, 31.63; H, 2.28; N, 5.27; S, 24.13. Found: C, 32.22; H, 2.52; N, 5.20; S, 24.67%; μeff (BM): 0.35.

(4) [Ni(L^2)$_2$]. Yield: 0.60g, 44%; M.Pt.: 215-217 °C; Selected FTIR, ν(cm^{-1}): 1508 (C=N), 1208 (C_2─N), 996 (C=S), 3001 (=C-H), 2917 (-C−H), 3185 (N-H), 411 (Ni–S); ^1H NMR ($CDCl_3$) δ, ppm: 7.0-7.4 (m, 10H, C_6H_5), 7.25(s, 2H, NH), 2.34 (s, 6H, CH_3); ^{13}C NMR ($CDCl_3$) δ, ppm: 123.5-128.9 (C_6H_5), 21.3 (CH_3), 196.5 (–CS_2); Anal calc for $C_{16}H_{16}N_2S_4Ni$ (423.26): C, 45.18; H, 4, 26; N, 6.59; S, 30.16; Found: C, 45.10; H, 4.23; N, 6.60; S, 30.20%; μeff (BM): 0.09.

(5) [Pd(L^2)$_2$]. Yield: 0.71g, 51%; M.Pt.: 230-233 °C; Selected FTIR, ν(cm^{-1}): 1511 (C=N), 1209 (C_2─N), 979 (C=S), 3032 (=CH−H), 2920 (H_2C−H), 3183 (N-H), 405 (Pd–S); ^{1}H NMR ($CDCl_3$) δ, ppm: 7.0-7.5 (m, 10H, C_6H_5), 9.68 (s, 2H, NH), 2.34 (s, 6H, CH_3). ^{13}C NMR ($CDCl_3$) δ, ppm 123-137 (C_6H_5), 21.2 (CH_3), 207.2 (–CS_2); Anal calc for $C_{16}H_{16}N_2S_4Pd$ (470.99): C, 40.63; H, 3.84; N, 5.92; S, 27.11. Found: C, 40.54; H, 3.57; N, 5.90; S, 26.93%; μeff (BM): 0.18.

(6) [Pt(L^2)$_2$]. Yield: 0.64g, 55%; M.Pt.: 248-250 °C; Selected FTIR, ν(cm^{-1}): 1512 (C=N), 1210 (C_2─N), 974 (C=S), 3025 (=CH−H), 2980 (H_2C−H), 3180 (N-H), 420 (Pt–S); ^{1}H NMR ($CDCl_3$) δ, ppm: 7.09-7.50 (m, 10H, C_6H_5), 9.64 (s, 2H, NH), 2.30 (s, 6H, CH_3); ^{13}C NMR ($CDCl_3$) δ, ppm: 123-137 (C_6H_5), 21.04 (CH_3), 210.0 (–CS_2). Anal calc for $C_{16}H_{16}N_2S_4Pt$ (559.66): C, 34.21; H, 3,23; N,4.99; S, 2.83. Found: C, 34.03; H, 3.43; N, 5.03; S, 2.75%; μeff (BM): 0.22.

(7) [Ni(L^3)$_2$]. Yield: 0.50 g, 83 %; M.Pt.: 209-212 °C; Selected FTIR, ν(cm^{-1}): 1533 (C=N), 1298 (C_2─N), 1019 (C=S), 3205 (=CH−H), 2961 (H_2C−H), 3205 (N-H), 442 (Ni–S); ^{1}H NMR ($CDCl_3$) δ, ppm: 6.50-7.18 (m, 10H, C_6H_5), 8.31 (s, 2H, NH), 1.25 (t, 6H, CH_3), 2.6 (q, 4H, CH_2); ^{13}C NMR ($CDCl_3$) δ, ppm: 115.0-129.0 (C_6H_5), 14.5 (CH_3), 28.2 (CH_2), 220.0 (–CS_2). Anal. calc for $C_{18}H_{22}N_2S_4Ni$ (453.33): C, 47.70; H, 4.89; N, 6.19; S, 28.29. Found: C, 47.20; H, 4.45; N, 6.60; S, 28.65%; μeff (BM): 0.10.

(8) [Pd(L^3)$_2$]. Yield: 0.56 g, 84 %; M.Pt.: 240-243 °C; Selected FTIR, ν(cm^{-1}): 1535 (C=N), 1298 (C_2─N), 1018 (C=S), 3206 (=CH−H), 2961 (H_2C−H), 3208 (N-H), 419(Pd– S); ^{1}H NMR ($CDCl_3$) δ, ppm: 6.80-7.30 (m, 10H, C_6H_5), 8.40 (s, 2H, NH), 5.90 (t, 6H, CH_3), 7.30 (q, 4H, CH_2); ^{13}C NMR ($CDCl_3$) δ, ppm: 120.0-145.0 (C_6H_5), 20.8 (CH_3), 45.2 (CH_2), 185.0 (–CS_2). Anal. calc. for $C_{18}H_{22}N_2S_4Pd$ (501.06): C, 43.15; H, 4.43; N, 5.59; S, 25.59. Found: C, 43.50; H, 4.80; N, 5.30; S, 25.31%; μeff (BM): 0.25.

(9) [Pt(L^3)$_2$]. Yield: 0.45g, 61 %; M.Pt.: 248-250 °C; Selected FTIR, ν(cm^{-1}): 1534 (C=N), 1298 (C_2─N), 964 (C=S), 3205 (=CH−H), 2961 (H_2C−H), 2961, 3205 (N-H), 419 (Pt-S); ^{1}H NMR (CDCl3) δ, ppm: 7.16-7.78 (m, 10H, C_6H_5), 8.44 (s, 2H, NH), 1.25 (t, 6H, CH_3), 2.65 (q, CH_2). ^{13}C NMR ($CDCl_3$) δ, ppm: 120.50-144.07 (C_6H_5), 15.73 (CH_3), 27.74 (CH_2), 179.30 (–CS_2). Anal. calc. for $C_{18}H_{22}N_2S_4Pt$ (589.72): C, 36.66; H, 3.16; N, 4.75; S, 21.74; Found: C, 36.20; H, 3.35; N, 4.20.; S, 21.20%; μeff (BM): 0.29.

2.4 X-ray crystallography

Data collection, structure solution and refinement for [Pt(L^1)$_2$], [Pt(L^3)$_2$] and [Pd(L^1)$_2$]

Pale yellow crystals with approximate dimensions 0.069 × 0.231 × 0.287, 0.086 × 0.134 × 0.282 and 0.256 x 0.374 x 0.473 mm^3 were used for [Pd(L^1)$_2$], [Pt(L^1)$_2$] and [Pt(L^3)$_2$] respectively. They were selected under oil in ambient conditions and attached to the tip of a MiTeGen MicroMount©. The crystals were each mounted in a stream of cold nitrogen at 100(2) K and centred in the X-ray beam using a video camera. The crystal evaluation and data collection were performed on a Bruker APEXII CCD DUO diffractometer with Mo K_α (λ = 0.71073 Å) radiation and the diffractometer to crystal distance was 6.00 cm [13]. The initial cell constants were obtained from three series of ω scans at different starting angles. Each series consisted of 12 frames collected at intervals of 0.5º in a 6º range about ω, with an exposure time of 10 seconds per frame. The reflections were successfully indexed by an automated indexing routine built in the APEX2 program suite. The final cell constants were calculated from a set of 6500, 6351 and 9210 strong reflections for [Pd(L^1)$_2$], [Pt(L^1)$_2$] and [Pt(L^3)$_2$] respectively from the actual data collection. The data were collected using a calculated set of parameters for the collection routine, consisting of ω and φ scans to survey the reciprocal space to the extent of a resolution of 0.75 Å. A total of 26240, 25200 and 15653 data for [Pd(L^1)$_2$], [Pt(L^1)$_2$] and [Pt(L^3)$_2$] respectively were harvested with exposure times of 10 sec per frame. These highly redundant datasets were corrected for Lorentz and polarization effects. The absorption correction was based on fitting a function to the empirical transmission surface as sampled by multiple equivalent measurements [14]. The systematic absences in the diffraction data were uniquely consistent for the space group *Pbca*, that yielded chemically reasonable and computationally stable results of refinement [15-20]. A successful solution by Intrinsic phasing methods (*SHELXT* [5]) provided all non-hydrogen atoms from the *E*-map. The remaining hydrogen atoms were located in an alternating series of least-squares cycles and difference Fourier maps. All non-hydrogen atoms were refined with anisotropic displacement coefficients. All hydrogen atoms connected to C atoms were included in the structure factor calculation at idealized positions and were allowed to ride on the neighbouring atoms with relative isotropic displacement coefficients. There is one symmetry-independent molecule in the asymmetric unit, consisting of one half of the Pd(II) complex for [Pd(L^1)$_2$], and a Pt(II) complex for [Pt(L^1)$_2$] and [Pt(L^3)$_2$]. The palladium and platinum metals are in the +2 oxidation state and charge balance comes from the bound

dithiocarbamate molecule connected by only two S atoms (S1 and S2) where the negative charge is localized on the S1 and S2 atoms. The other half of the molecule is generated by symmetry with the Pd and Pt atoms (Figure 1) residing on a special position (0.5, 0, 0.5). The final difference Fourier map was basically featureless for both structures.

2.5 Computational details

DFT calculation studies

Density functional theory (DFT) calculations were carried out using the Gaussian 2009 program suite [21] on the high performance computing facility at the University of Waikato. Unless otherwise specified, all DFT calculations were completed using the 6-311G+(d,p) basis set for all main group elements and the LANL2DZ basis set and effective core potential (ECP) for Pt, Pd and Ni atoms. Geometry optimizations and harmonic frequency calculations in the gas phase were run with the B3LYP functional using the default optimization criteria. The absence of imaginary frequencies in the calculated vibrational frequencies of the ligands and complexes showed that the optimized geometries were minima. The geometries of the ligands were also re-optimized using three different density functionals, B3LYP, ωB97XD and M06-2X, in the presence of an implicit solvent [22]. The frontier molecular orbital energies and reactivity indicators of the ligands and complexes were calculated. Natural Bond Orbital (NBO) calculations were implemented on the complexes using the CAM-B3LYP functional. Non-covalent interaction (NCI) theory calculations were implemented on the hydrogen bonded structures of palladium and platinum. The initial input geometries were adapted from the crystal structures of the compounds and carried out using the ωB97XD functional. The NCI iso-surfaces were generated using Bonder, a locally written software program, with visualisation using VMD.

2.6 Antimicrobial studies

The microbes were clinical isolates collected from the Department of Microbiology, Federal Teaching Hospital, Abakaliki, Nigeria. They included Gram negative (*Escherichia coli*, *Klebsiella Pneumonia* and *Pseudomonas Aeruginosa*), Gram positive (*Bacillus cereus* and *Staphylococcus aureus*) and fungi (*Candida albicans* and *Aspergillus flavus*) organisms. The choices of the microbial strains were based on their clinical and pharmacological relevance [23]. The agar disc diffusion method [24] was utilized for the antimicrobial screening.

Sterile Muller–Hinton agar (MHA) was prepared and poured on petri plates. A standard method was adopted for the microbial culture using 80% dimethylsulfoxide as the solvent and 1.25 mg/mL 3-(4,5-dimethylthiazol-2-yl)-2, 5-diphenyltetrazolium bromide (MTT) to monitor the occurrence of a purple colouration [25]. A commercially available antibacterial drug (Sulfamethoxazole) and an antifungal drug (Ketoconazole) were used as the positive control drugs, while 80% dimethylsulfoxide was used as a negative control under similar conditions. Measurements were conducted four times and the experimental results were given as the mean ± S.D. of all the measurements.

3. Results and discussion

3.1 Synthesis

Scheme 1 presents the preparation of the ligand, which proceeded in the presence of a strong alkaline solution (ammonium hydroxide or sodium hydroxide) at a very low temperature (in ice). All the complexes were prepared using the direct reaction of solutions of the metal salts and ligands in a 1:2 stoichiometric ratio at room temperature. All the complexes formed are intensely coloured, as expected for d^8 transition metals (due to *d-d* transitions), with different shades of green for the nickel, orange for the palladium and yellow for the platinum complexes. They are all insoluble in water, but soluble in different low boiling point organic solvents such as chloroform, dichloromethane and methanol.

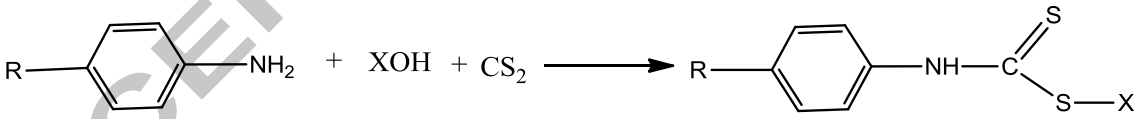

1. R=H; X=NH_4
2. R=CH_3, C_2H_5; X= Na

Scheme 1: Preparation of the dithiocarbamate ligands.

3.2 Infra-red spectral studies

The FT-IR spectra of the dithiocarbamate compounds show characteristic bands within the 1450-1580 cm^{-1} region, due to the stretching vibration of the thioureide band ν (N=CS_2), and the 950-1050 cm^{-1} region, assigned to a ν(C-S) vibration [26]. The spectral data were compared and assigned based on similar reported compounds in the literature [27, 28]. The FTIR spectra of the ligands gave intense stretching vibrational bands for their thioureide

groups at 1452, 1507 and 1508 cm^{-1} for L^1, L^2 and L^3 respectively, which shifted to higher wavenumbers in the spectra of the metal complexes. The increase in wavenumber of the C=N bands compared to those obtained in the spectra of the free ligands could be attributed to the chelation of the sulfur atoms to the metal ions, which reinforces the double bond character of the C=N group by strengthening the force constant of the bond, thus giving a higher wavenumber [29]. In addition, the vibration bands for *ν*(C= N) increase from Ni to Pt due to the increase in the Lewis acid properties of the metals. The π-donor property also gets weaker down the group 10 metals, thus raising the C=N vibrations [30]. The effect of the strength of the electron donating substituents (H, CH_3 and CH_2CH_3) in the *para* position of the phenyl ring was observed as the values of the thioureide bands appeared in the order $L^1 < L^2 < L^3$. The *ν*(C–S) vibrational band was observed as a single band around 1018-1040 cm^{-1} in the spectra of the ligands, and it appeared at relatively lower wavenumbers in the complexes. The single band indicated a symmetrical bidentate coordination of the ligand to the metal center [30]. The magnitude of the C-S bands were also in the order $L^1 < L^2 < L^3$.

3.3 NMR spectroscopic studies

The NMR spectra of the ligands showed the protons of the phenyl ring as multiplets in the range δ 6.96-7.88 ppm. The peaks were slightly higher in the spectra of the metal complexes. The increase in chemical shift could be attributed to a weak deshielding brought about by the shift of electron density towards the nitrogen atom of the NHR′ group, thereby enhancing the electron density on the sulfur atom via the thioureide π-system [31]. The NH proton peaks appeared at δ 10.12-10.10 ppm for the uncoordinated ligands but were deshielded to lower chemical shifts in the spectra of the complexes. The ^{13}C NMR spectra exhibited peak values within the expected range, but in different environments. In the spectra of the uncoordinated ligands the -NCS_2 peak positions were observed at δ 196.1, 196.5 and 179.3, ppm for L^1, L^2 and L^3 respectively. These peaks resonated around δ 196.7-220.0, 196.7-206.9, 196.9-210 ppm in the spectra of the Ni(II), Pd(II) and Pt(II) complexes. An increase in the -NCS_2 peak position is generally observed down the group of each series, confirming that the heavier atom complexes have higher *δ* values than the lighter atoms in the same group [31].

3.4 X-ray crystallography studies

The X-ray structures of the bis-(*N*-phenyldithiocarbamate)palladium(II), bis-(*N*-phenyldithiocarbamate)platinum(II), and bis-(4-ethylphenyldithiocarbamate)platinum(II) complexes are presented in Figure 1, and their crystal and structure refinement data are summarized in Tables 1 and 2. The coordination environment of the Pd complex shows symmetric bond lengths with the Pd-S distances Pd(1)-S(1) = 2.3232(5) Å and Pd(1)-S (2) = 2.3399(5) Å. In bis-(*N*-phenyldithiocarbamate)platinum(II) and bis-(4-ethylphenyldithiocarbamate)platinum(II) complexes, symmetric bond lengths were also exhibited with Pt-S distances Pt1-S1=2.3201(7) Å and Pt1-S 2=2.3313(7) Å in the former; and Pt(1)-S(1) = 2.3163 (6) and Pt(1)-S(2) = 2.3216 (6) Å in the later. All the complexes have a distorted square planar geometry due to the small S-Pd/Pt-S2 bite angles of 75.134(17), 74.75(3) and 74.93 (2)° for $[Pd(L^1)_2]$, $[Pt(L^1)_2]$ and $[Pt(L^3)_2]$, respectively. The phenyl groups make angles of 86.17(7) and 86.03(7)° with the dithiocarbamate planes in the palladium complex, $[Pd(L^1)_2]$. However, in the Pt complex $[Pt(L^1)_2]$, analogous angles of 87.20(10) and 86.95(10)° were made; while in $[Pt(L^3)_2]$ they were 87.40(8) and 87.47(9) °. The bond lengths for both Pd-S and Pt-S are relatively close, 2.32-2.34 and 2.32-2.33 Å. Comparing the Pt-S bond lengths in $[Pt(L^1)_2]$ (2.3201-2.3202 Å), with an unsubstituted phenyl group in the ligand L^1, and the Pt-S bond lengths in $[Pt(L^3)_2]$ (2.3163-2.3216 Å), where the ligand L^3 bears a *p*-ethylphenyl group, there is a slight variation. The bond lengths were slightly reduced by the presence of the ethyl group, which may influence the intramolecular interactions between the atoms. However, their intermolecular hydrogen bonding interactions are similar (details of which appear in Table 3 for $[Pd(L^1)_2]$, Table 4 for $[Pt(L^1)_2]$, and Table 5 for $[Pt(L^3)_2]$; selected interactions are also shown in Figure 1), which supports their similar coordination modes and chemical properties and also explains why they are usually studied as a group [32].

3.5 Thermal studies of the compounds

Figures 2-4 show the overlapped TGA/DTG graphs of the complexes. Relevant data from the decomposition are presented in Table 6. The metal complexes show similar single step decomposition patterns in the range 163-294 °C. The Ni and Pd complexes of the ligand L^1 resulted in residues with a mass of 2.78/2.60 and 3.84/4.10 mg (calculated/found,) respectively, indicating a 1:1 ratio of the metal to sulfide ((NiS and PdS). The $[PtL^1_2]$ complex yielded a 1:2 metal to sulfur ratio with a residual mass of 5.66/5.57 mg, which confirmed PtS_2. The metal complexes of the ligands L^2 and L^3 followed a similar pattern of

single step decomposition, with the onset around 114 and 174 °C, which proceeded up to 295 and 423 °C, respectively, with various percentage weight losses. All the obtained residues conformed to a 1:1 metal-sulfur ratio, indicating NiS, PdS, and PtS. The presence of the methyl and ethyl substituents on the phenyl ring increased the thermal stability of the complexes and the stability increased in the order $L^3 > L^2 > L^1$. To show the variation in the temperature of the maximum rate of decomposition between complexes of the same ligand moiety, their respective DTG graphs were overlapped. Figures 2b, 3b and 4b present the overlapped DTG graphs which conspicuously show the changes in their decomposition peaks as a function of the type of metal ions and also the ligand type. All the complexes are potential single source precursors for the synthesis of their respective metal sulfide nanoparticles [33].

3.6 Antimicrobial studies

The compounds were screened at the three different concentrations of 10, 25 and 50 µg/mL. Significant zones of inhibition were obtained at 50 µg/mL and these were taken as the minimum inhibitory concentration of the metal complexes against the microbes: Gram positive (*S. Aureus* and *B. cerues*), Gram negative (*K. pneumonia, P. aeruginosa* and *E. coli*) and two fungi organisms (*C. albican* and *A. flavus*). The results are presented in Table 7.

The metal complexes gave varied antimicrobial activities which ranged from moderate to very active. *E. Coli* was susceptible to all the complexes, while *P. Aeruginosa* and *K. Pneumonia* were susceptible to all the complexes except for $[Pd(L^1)_2]$ and $[Ni(L^2)_2]$ respectively. In general, the Gram negative bacteria organisms were more vulnerable to the complexes as compared to the Gram positive bacteria organisms. This is probably due to the presence of an outer protective lipopolysaccharide membrane in Gram positive bacteria strains which does not permit lipophobic materials into the cell, making penetration of the complexes intricate [34]. However, the metal complexes of L^3 were mostly very active against both Gram positive and Gram negative bacterial strains. They were the most active of the metal complexes screened against the microbes.

The compounds displayed better antibacterial activity compared to their antifungal activity. $[Pt(L^3)_2]$ had the best antifungal activity against *C. albican* and *A. flavus* compared to the other complexes, but lower activity than Ketoconazole, used as the standard drug. Similarly, Sulfamethoxazole exhibited the best antibacterial activity against all the bacteria strains

compared to the metal complexes except for $[Pt(L^3)_2]$ against *S. aureus*. In addition $[Pt(L^3)_2]$ exhibited 89, 82 and 77% of the antibacterial activity of Sulfamethoxazole against *B. cereus*, *P. aeruginosa* and *S. aureus*, respectively. The Ni(II) and Pd(II) complexes of L^2 and L^3 showed better antimicrobial activities compared to literature reports involving similar compounds [35]. Similarly, $[Pt(L^3)_2]$ exhibited better antibacterial properties compared to related literature studies [36]. Interestingly, the antimicrobial results of the metal complexes were better than those reported in literature [37, 38]. The compounds could be probable lead agents in antimicrobial research.

3.7 Computational studies

3.7.1 Molecular electrostatic potential (MEP)

The molecular electrostatic potential (MEP) is a three dimensional cloud around a molecule created by its nuclei and electrons. It is very helpful in predicting the reactivity of a range of chemical systems for both electrophilic and nucleophilic sites. A number of chemical interactions, including drug-receptor interactions, enzyme-substrate interactions and hydrogen bonding in both chemical and biological systems, are predicted with the use of molecular electrostatic potentials. The molecular electrostatic potential V(r) is represented as:

$$V(\acute{r}) = \sum_{A-1}^{M} \frac{Z_A}{|r - R_A|} - \int \frac{d\acute{r}\rho(r)}{|\acute{r} - r|}$$

where Z_A is the charge on the nucleus A located at R_A and ρ(r) is the electronic density function of the molecule obtained from its computed wave function. V(ŕ) is a real physical property that can be determined experimentally as well as computationally [21]. In order to investigate the reactive sites in the compounds, the molecular electrostatic potentials were evaluated at the B3LYP/6-311++G(d,p) level of theory. The values of the electrostatic potential at the surface are defined by different colours, with the potential increasing in the order from red < orange < yellow < green < light blue < blue. Figure 5 shows the electrostatic potential maps and contour diagrams for the dithiocarbamate ligands. The negative yellow regions of the MEP map are related to the negative electrostatic potential and sites for electrophilic attack. These regions are localized around the dithio functionality with potential values of -0.0585, -0.05836 and -0.06083 au for the three ligands L^1, L^2 and L^3,

respectively. The negative blue regions of the electrostatic potential map, on the other hand, are related to the nucleophilic reactivity and they are localized around the imine hydrogen atom of the dithiocarbamate with positive potential values of 0.0485, 0.0483 and 0.0508 au for L^1, L^2 and L^3, respectively. The electrochemical potential maps for the three ligands show that the dithio-group has the most positive electrostatic potential in the three ligands and, thus, is the most likely site for metal attack. There was also a slight increase in the electrostatic potential value with the increase in the alky substituent attached to the phenyl ring.

3.7.2. Frontier molecular orbital energies and chemical reactivity

The frontier molecular orbitals, which includes the highest occupied molecular orbital (HOMO) and the lowest unoccupied molecular orbital (LUMO), are very important quantum chemical parameters because they indicate the possibility of electronic transitions in molecules. They are crucial for the understanding of electron transfer processes in a molecule during chemical reactions [22]. The HOMO orbital primarily acts as the electron donor and the LUMO largely acts as the electron acceptor, and the gap between the HOMO and LUMO determines the chemical stability of the molecule [39]. The HOMO and LUMO orbital diagrams for the three dithiocarbamate ligands are presented in Figure 6. The orbital diagrams show that the HOMO orbitals are located on one of the sulfur atoms of the dithiocarbamate ligand, while the LUMO orbitals are located on the dithiocarbamate carbon atom for all three ligands. This is an indication of electron donation from the occupied sigma orbitals of the sulfur atom to the unoccupied π orbitals of the carbon atom. The HOMO-LUMO energy gap can be used as a stability index, providing an estimation of the reactivity of the molecule [22]. A large HOMO-LUMO energy gap indicates high stability and low chemical reactivity. A smaller energy gap indicates less stability and higher reactivity of the molecule and, thus, an easier electronic transition [21, 40]. The values of the HOMO-LUMO energy gap presented in Table 8 show a low energy gap at the B3LYP level of theory and this increases as the density functional changes from B3LYP to M062X, and then to ωB97XD. The nature of the alkyl substituent on the phenyl ring of the dithiocarbamate ligands did not have any significant effect on the reactivity of the molecules. Apart from the HUMO and LUMO energies, there are other reactivity descriptors that can be obtained from the HOMO-LUMO relationship. The global reactivity descriptors based on Koopmans theorem [41]

include the ionisation potential (IP), electron affinity (EA), chemical potential (μ) and the chemical hardness (η). The global electrophilicity index (ω), proposed by Parr *et al* [42], was also evaluated. Lower values of the chemical hardness, electrophilicity index and chemical potential are related to better electron donating properties. The chemical reactivity parameters for the dithiocarbamate ligands using three different functionals were investigated and the results are presented in Table 8. The results indicate no significant effect of using different functionals on the reactivity parameters. Small values of the chemical hardness η are an indication of the dominance of the electron donating properties of the ligands. There is, however, no significant difference in the chemical hardness as the substituent at the *para* position of the phenyl ring of the dithiocarbamate ligand increased from H, to CH_3 and then to C_2H_5 across the three levels of theory. The implication of this is that the three dithiocarbamate ligands are of similar reactivity and the size or nature of the alkyl substituent on the phenyl group has little or no significant effect on the kinetic stability of the compounds.

The frontier molecular orbital molecular orbital diagrams for the complexes are also presented in Figure 7, and the energy gap and reactivity parameters are presented in Table 9. The molecular orbital diagrams show that the HOMO orbitals are located around the metal coordination environment for all the complexes while the LUMO orbitals are spread around most of the compound for the platinum complexes. The LUMO orbitals for the palladium and nickel complexes are also concentrated around the metal coordination area. The orbital diagrams and the reactivity parameters in Table 9 show a lot of similarities in the metal complexes formed from the three dithiocarbamate ligands.

3.7.3. Non-covalent interactions in the hydrogen bonded platinum and palladium complexes

The supramolecular architecture of a compound in the solid state is a function of the nature and strength of the different non-covalent interactions in the molecule [43]. These non-covalent interactions, which may include hydrogen bonding, halogen bonding, Van der Waals or dipole-dipole interactions, are dependent on the electron density around the compound. A number of topological methods can be applied in order to identify the relationship between the electron density and molecular reactivity [44-46]. Non-covalent interaction (NCI) theory is based on analysis of the reduced density gradient, which is represented as:

$$s = \frac{1}{2(3\pi^2)^{1/3}} \frac{|\nabla\rho|}{\rho(\mathbf{r})^{4/3}}$$

Non-covalent interactions are revealed by regions where the reduced density gradient is small and the density is low but non-negligible. [47]. The reduced density gradient is plotted as a function of the electron density ρ, oriented by the sign of λ_2 to identify the interaction types. Attractive interactions appear at $\lambda_2 < 0$ while repulsive interactions appear at $\lambda_2 > 0$. A pictorial 3D representation of these interactions with an RGB (red-green-blue) colouring scheme is used to rank these interactions. Red represents strong repulsive/destabilizing interactions, which include ring closure interactions and steric interactions, while blue regions are associated with highly attractive/stabilizing interactions, including hydrogen bonding interactions. In between the two extremes are the green regions, indicating weaker van der Waals interactions. The 3D isosurface plot for the palladium dithiocarbamate complex is shown in Figure 8. The plot shows only the relevant intermolecular interactions that are responsible for the hydrogen-bonded chain found in the molecule. The strongest interaction found in the dimer is the strong stabilizing intermolecular hydrogen bonding interaction, shown as a blue pill-like isosurface between the dithiosulfur group of one complex and the N-H group of another complex. Similar intermolecular hydrogen bonding interactions were reported for a hydrogen bonded 2-{[2-(phenylsulfonyl) hydrazinylidene]methyl}benzoic acid dimer [46]. Another interaction, depicted in the palladium complex dimer in Figure 7, is the weak intermolecular n-π interaction, shown as a light green flat isosurface between the dithiosulfur group and the π bond of the adjacent phenyl ring. This interaction can be classified as van der Waals forces in terms of strength. Finally, the last interaction, with a large flat boat-shaped isosurface, has a mixture of a slightly attractive green coloured Van der Waals interaction from the intermolecular Pd-S interaction and a slightly repulsive yellow coloured interaction resulting from intermolecular S–S interaction. Similar interactions were found for the platinum dithiocarbamate complex (picture not shown).

3.7.4 Natural Bond Orbital (NBO) analysis

The natural bond orbital theory is an explicit method of studying intermolecular and intramolecular interactions in a compound. It provides the basis for investigating the charge transfer and hyperconjugative interactions in a molecular system [48]. NBO analysis was carried out for the Pt, Pd and Ni dithiocarbamate complexes by examining the possible interactions between the filled orbitals (donor) Lewis type NBOs and the empty orbital

(acceptor) non-Lewis type NBOs. The hyperconjugative energy of this interaction can be estimated by second order perturbation theory [49]. The strength of the bond in a molecule can be estimated by the value of the stabilization energy E^2 which is a pointer to the level of interaction between the electron donor and the electron acceptor [50]. NBO analysis for the six dithiocarbamate complexes was performed with the CAM-B3LYP functional. Selected donor acceptor interactions and their stabilization energies are presented in the supplementary Table S1. The table shows a number of donor – acceptor interactions from the σ lone pair orbitals of the sulfur atom to the π* orbitals of the conjugated dithiocarbamate carbon atom, with the highest stabilization energies ranging from 153 to 201 kcal/mol in all the complexes. This is an indication of electron delocalisation in the complexes. The other donor-acceptor interactions with high stabilization energies of between 162 and 180 kcal/mol are the n–π* interactions. The n–σ* (LpS - LP*M, M = metal) interactions, with stabilizations energies of 5.5 − 7.7 kcal/mol, are also prominent in all the metal complexes. Apart from that, there are other π – π* (BDC – BD*C) interactions with high stabilization energies of between 18.0 and 25 kcal/mol, indicative of relative bond strength. Some strong metal to ligand charge transfer (MLCT) interactions were also recorded for the platinum dithiocarbamate complexes with high stabilization energies of between 10 and 20 kcal/mol.

Conclusion

The biological relevance of the acidic proton (NH) in dithiocarbamate derived from primary amines has motivated the synthesis of substituted and unsubstituted phenyldithiocarbamates. The ligands were obtained from *N*-phenylaniline, 4-methylaniline and 4-ethylaniline, which yielded dithiocarbamate ligands denoted as L^1, L^2 and L^3 respectively. Metal complexes of Ni(II), Pd(II) and Pt(II) were subsequently synthesized and characterised; quantum mechanical calculations were used to explore their bonding properties and interactions. NCI analysis of the complexes indicated the presence of strong stabilizing inter-molecular N-H---S hydrogen bonding and weaker intermolecular n---π and Pd---S van der Waals interactions. Frontier molecular orbital analysis indicated the delocalisation of electrons around the coordination sphere of the metal complexes and an increase in the length of the alkyl substituent on the phenyl groups showed no significant effect on the HOMO-LUMO energy gaps. The high stabilisation energies of the metal complexes from second order perturbation analysis of the fork matrix in the NBO is an indication of a very strong metal-ligand

interaction for the complexes. The antimicrobial results showed that antimicrobial activities followed the order $L^1 < L^2 < L^3$ (for their metal complexes). The ethyl substituted dithiocarbamate complexes had the best antimicrobial activity compared to the unsubstituted and methyl substituted dithiocarbamate complexes. These compounds could be probable lead agents in antimicrobial research.

Supplementary data

Crystallographic data of the complexes have been deposited with the Cambridge Crystallographic Data Center allocated with the deposit numbers CCDC 1849649, 1848912 and 1875081. Copy of the data can be obtained free of charge on application to CCDC, 12 Union Road, Cambridge CB2 1EZ, UK, fax: +44 1223 336033, email:deposit@ccdc.cam.ac.uk.

REFERENCES

[1] A. C. Ekennia, A. J. Odola, Inter. J. Pharm. Bio. Chem. Sci. 2 (2013) 21.

[2] D.C. Onwudiwe, P.A. Ajibade, Mater. Lett. 65 (2011) 3258.

[3] K. Ghosh, V. Mohan, P. Kumar, S.W. Ng, E.R.T. Tiekink, Inorg. Chim. Acta. 416 (2014) 76.

[4] D.E. Lynch, I. McClenaghan, Cryst. Eng. 6 (2003) 1.

[5] K.C. Chang, S.S. Sun, M.O. Odago, A.J. Lees, Coord. Chem. Rev. 284 (2015) 111.

[6] A. C. Ekennia, J. Applied Chem. *(IOSR-JAC)*, 5 (2013) 36.

[7] G. Hogarth. Transition Metal Dithiocarbamates: 1978–2003. (2005) 53. Ed. Kenneth D. Karlin.in. Progress in Inorganic Chemistry. Wiley

[8] F. Fu, H. Zeng, Q. Cai, R. Qiu, J. Yu, Y. Xiong, Chemosphere 69 (2007) 1783.

[9] S. Kanchi, P. Singh, K. Bisetty, Arab. J. Chem. 7 (2014) 11.

[10] G .Hogarth, Mini Rev. Med. Chem. 12 (2012) 1202.

[11] V. Bala, G. Gupta, V. L. Sharma. Mini Rev. Med. Chem. 14 (2014) 1021.

[12] D. C. Onwudiwe, A. C. Ekennia. Res Chem. Intermed. 43 (2017) 1465.

[13] Bruker-AXS (2014). *APEX2*. Version 2014.11-0. Madison, Wisconsin, USA.

[14] L. Krause, R. Herbst-Irmer, G. M. Sheldrick, D. Stalke, J. Appl. Cryst. 48 (2015) 3.

[15] G. M. Sheldrick, (2013). *XPREP*. Version 2013/1. Georg-August-Universität Göttingen, Göttingen, Germany.

[16] G. M. Sheldrick, Acta Cryst. D66 (2010) 479.

[17] G. M .Sheldrick, Acta Cryst. A71 (2015) 3.

[18] G. M. Sheldrick, Acta Cryst. C71 (2015) 3.

[19] O. V. Dolomanov, L. J. Bourhis, R. J. Gildea, J. A. K. Howard, H. Puschmann, J. Appl. Cryst. 42 (2009) 339.

[20] I. A. Guzei, (2007-2013). Programs Gn. University of Wisconsin-Madison, Madison, Wisconsin, USA.

[21] A. Zülfikaroğlu, H. Batı, N. Dege, J. Mol. Struct. 1162 (2018) 125.

[22] A.O. Zacharias, A. Varghese, K. Akshaya, M. Savitha, L. George, J. Mol. Struct. 1158 (2018) 1.

[23] W.P. Ross, P.W. Malbrook, Clinical and oral microbiology, Hemispher Publishing Corporation, New York, 1982.

[24] M. Balouiri, M. Sadiki, S.K. Ibnsouda, J. Pharm. Anal. 6 (2016) 71.

[25] H.J. Simon, E.J. Yin, Appl. Envir. Microbiol. 19 (1970) 573.

[26] A. Manohar, K. Karpagavel, A. Murugan, Int. J. Chem. Tech. Res. 6 (2014) 474.

[27] J. P. Fuentes-Martínez, I. Toledo-Martínez, P. Román-Bravo, P.G.y. García, C. Godoy-Alcántar, M. López-Cardoso, H. Morales-Rojas, Polyhedron 28 (2009) 3953.

[28] N. Singh, S. Bhattacharya, J. Organomet. Chem.700 (2012) 69.

[29] J. O. Adeyemi,, D. C. Onwudiwe, A. C. Ekennia, R. C. Uwaoma, E. C. Hosten.. Inorg. Chim. Acta 477 (2018) 148.

[30] E. Sathiyaraj, G. Gurumoorthy, S. Thirumaran, New J. Chem. 39 (2015) 5336.

[31] B.A. Prakasam, K. Ramalingam, G. B. Andrea, Polyhedron 26 (2007) 4489.

[32] A. L. Spek, Acta Cryst. D65 (2009) 148.

[33] D. C. Onwudiwe, J. N. Mugo, H. Madalina, H. Eric, J. Sulfur Chem. 36 (2015) 36.

[34] F. Javed, M. Sirajuddin, S. Ali, N. Khalid, M.N. Tahir, N.A. Shah, Z. Rasheed, M.R. Khan, Polyhedron 104 (2016) 80.

[35] S. I. Islam, S. B. Das, S. Chakrabarty, S. Hazra, A. Pandey, A. Patra. Adv. Chem. 2016 (2016) 1.

[36] M. Mijajlovic, S. Vasic, I. Radojevic, J. Maksimovic, L. Comic, M. Nikolic, G. Radic. 2nd international electronic conference on medicinal chemistry (2016).

[37] P. A. Ajibade, O. G. Idemudia, A. I. Okoh, Bull. Chem. Soc. Ethiop. (2013) 27.

[38] M. Gaber, H. A. El-Ghamry, M. A Mansour. J. Photochem. Photobio. 354A (2018) 163.

[39] A. Eşme, S.G. Sağdınç, Acta A188 (2018) 443.

[40] V. Balachandran, M. Murugan, V. Karpagam, M. Karnan, G. Ilango, Spectrochim. Acta, 130A (2014) 367.

[41] T. Koopmans, Physica 1 (1934) 104.

[42] R.G. Parr, L.v. Szentpaly, S. Liu, J. Am. Chem. Soc. 121 (1999) 1922.

[43] E.E. Oyeka, J.N. Asegbeloyin, I. Babahan, B. Eboma, O. Okpareke, J. Lane, A. Ibezim, H.H. Bıyık, B. Törün, D.C. Izuogu, J. Mol. Struct. 1168 (2018) 153.

[44] J. Cioslowski, S.T. Mixon, J. Am. Chem. Soc. 114 (1992) 4382.

[45] B. Silvi, A. Savin, Nature 371 (1994) 683.

[46] J.N. Asegbeloyin, D.C. Izuogu, E.E. Oyeka, O.C. Okpareke, A. Ibezim, J. Mol. Struct. 1175 (2019) 219.

[47] J.N. Asegbeloyin, E.E. Oyeka, O. Okpareke, A. Ibezim, J. Mol. Struct. 1153 (2018) 69.

[48] F. Weinhold, C.R. Landis, Chem. Educ. Res. Prac.2 (2001) 91.

[49] J. Chocholoušová, V. Špirko, P. Hobza, Phys. Chem. Chem. Phys. 6 (2004) 37.

[50] M.K. Awad, M.F. Abdel-Aal, F.M. Atlam, H.A. Hekal, Spectrochim. Acta 206A (2019) 78.

Figures

(**a**)

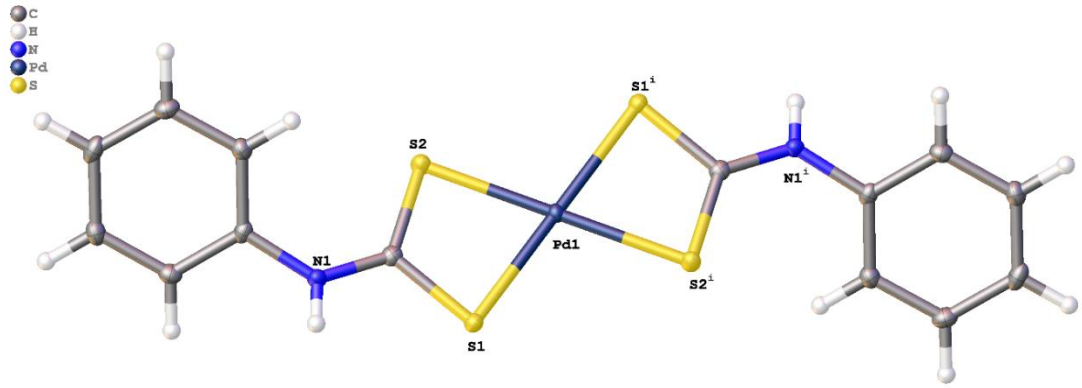

(**b**)

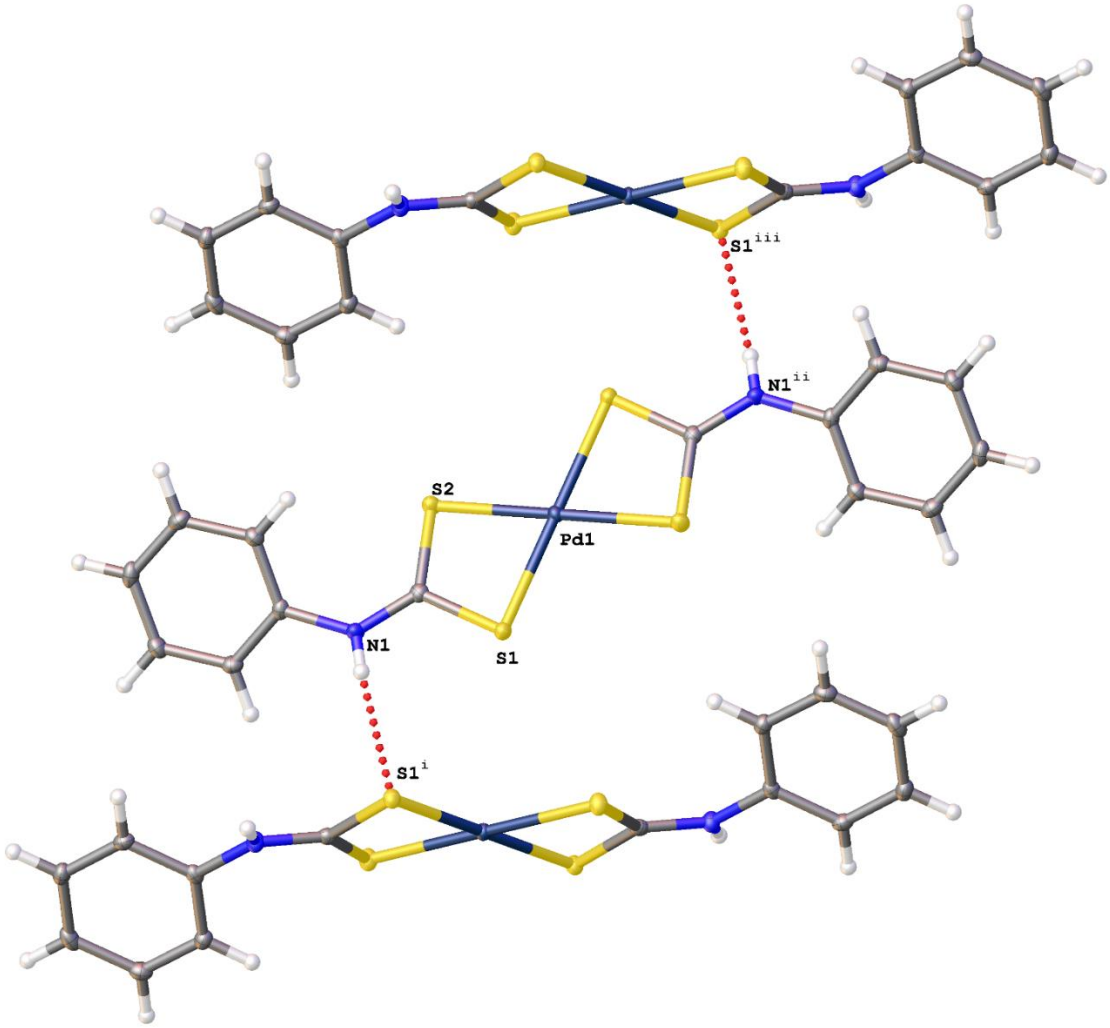

(c)

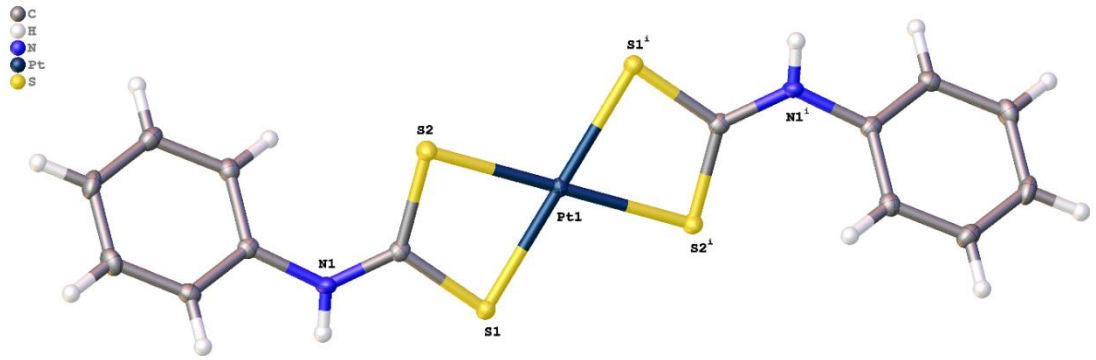

(d)

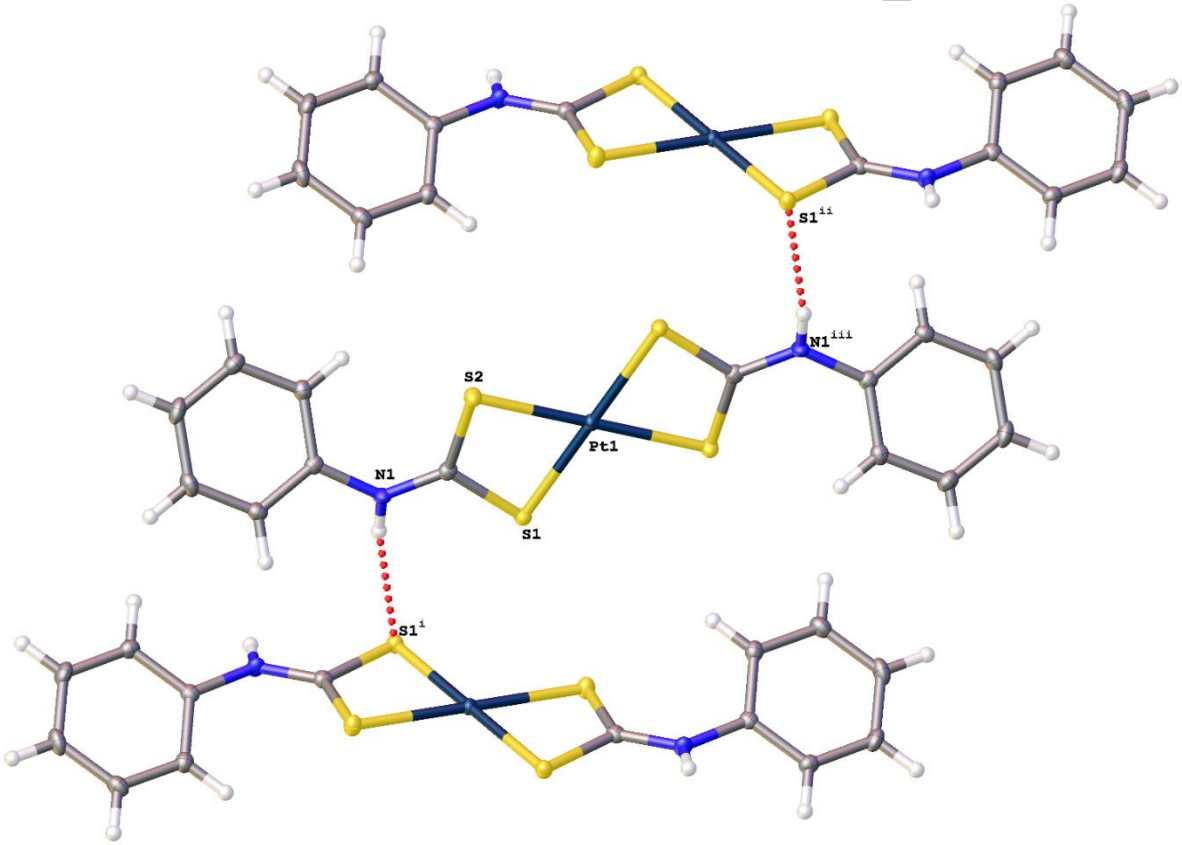

(**e**)

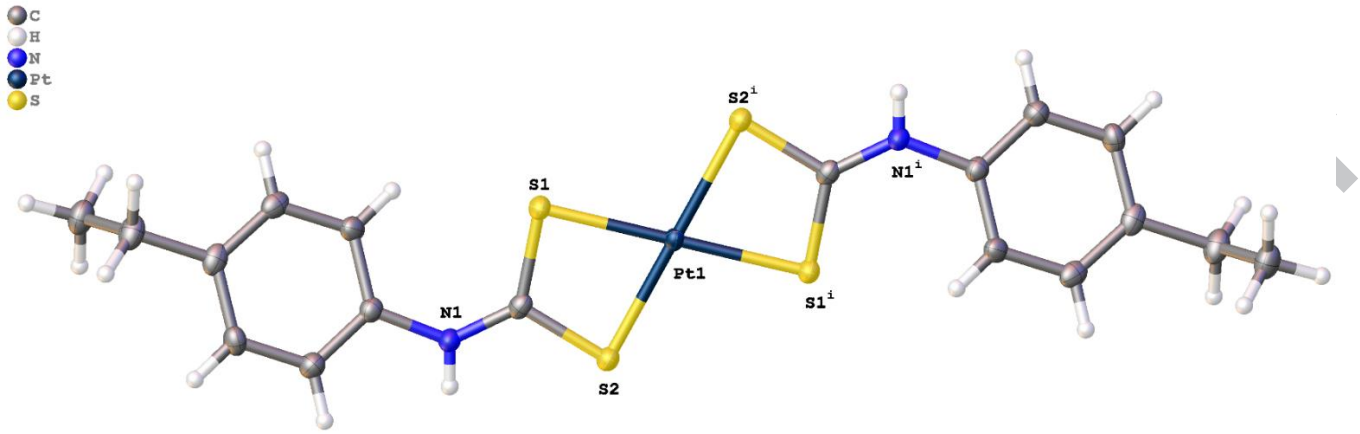

(**f**)

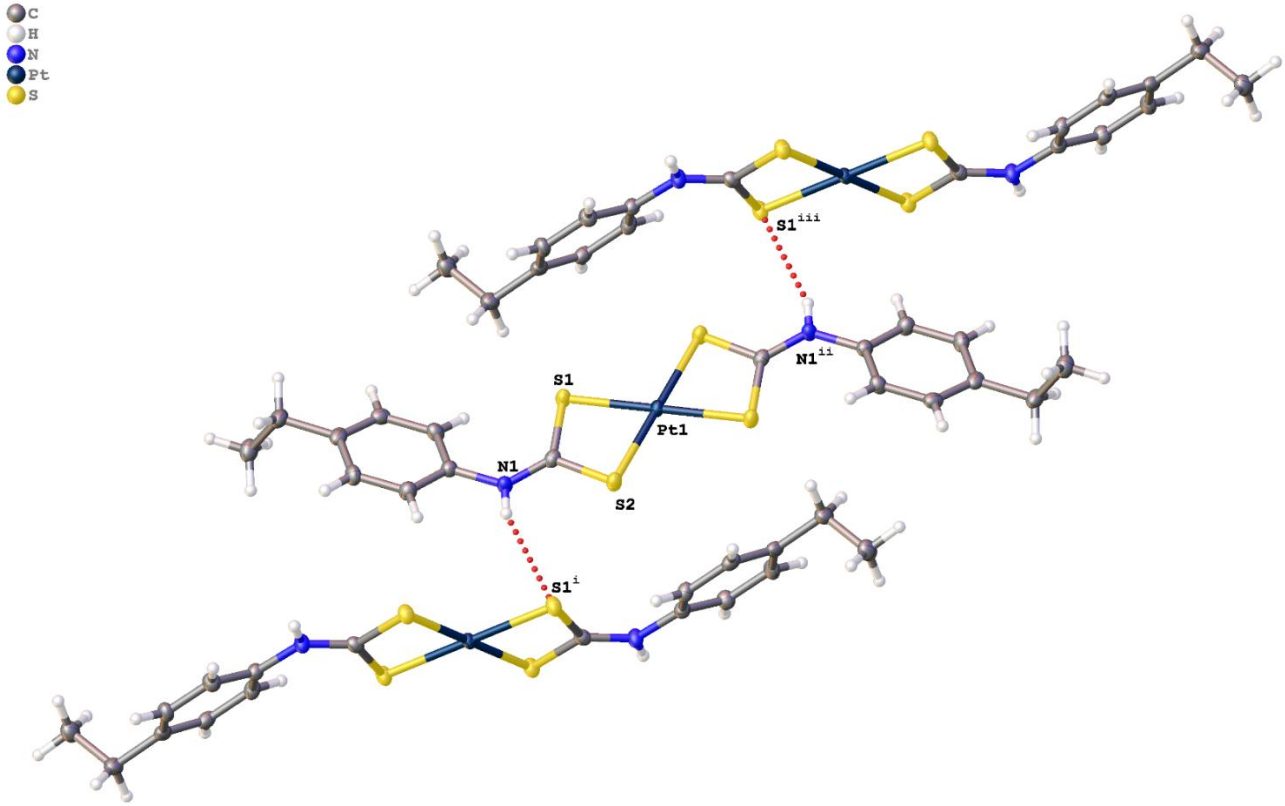

Fig 1: (a) Molecular structure of $[Pd(L^1)_2]$ with atomic displacement ellipsoids drawn at the 50% probability level; (b) intermolecular hydrogen bonding contacts of $[Pd(L^1)_2]$; (c) molecular structure of $[Pt(L^1)_2]$ with atomic displacement ellipsoids drawn at the 50% probability level; (d) intermolecular hydrogen bonding contacts of $[Pt(L^1)_2]$; (e) molecular structure of $[Pt(L^3)_2]$ with atomic displacement ellipsoids drawn at the 50% probability level; (f) intermolecular hydrogen bonding contacts of $[Pt(L^3)_2]$. In all three diagrams, the N–H···S interactions are also shown as red dashed lines and symmetry positions for all three structures are identical at: (i) 3/2–*x*, ½+*y*, *z*, (ii) 1–*x*, –*y*, 1–*z*, (iii) –½+*x*, –½–*y*, 1–*z*

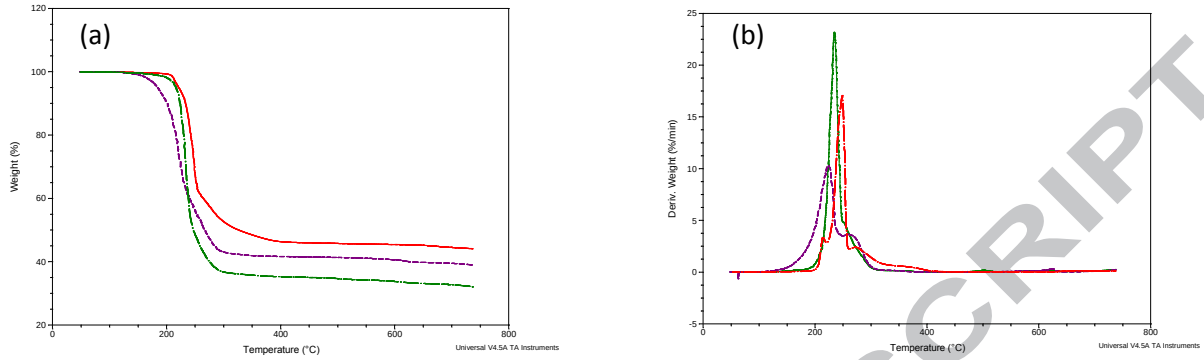

Fig.2: (a) TG and (b) DTG of the Ni (green), Pd (purple) and Pt (red) complexes of L^1

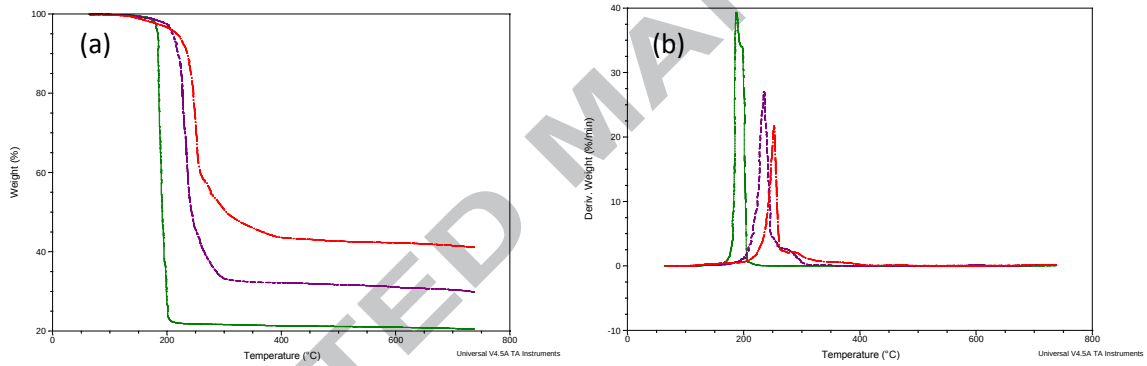

Fig.3. (a) TG and (b) DTG of the Ni (green), Pd (purple)and Pt (red) complexes of L^2

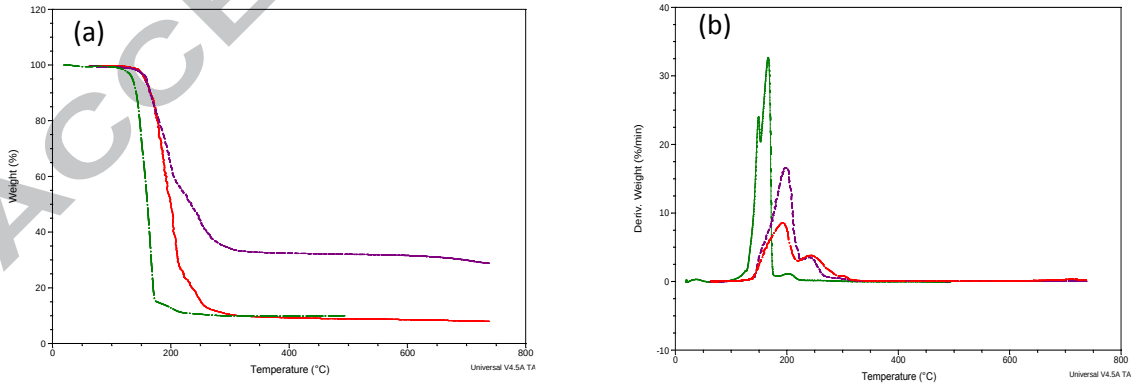

Fig.4: (a) TG and (b) DTG of the Ni (green), Pd (purple), and Pt (red) complexes of L^3

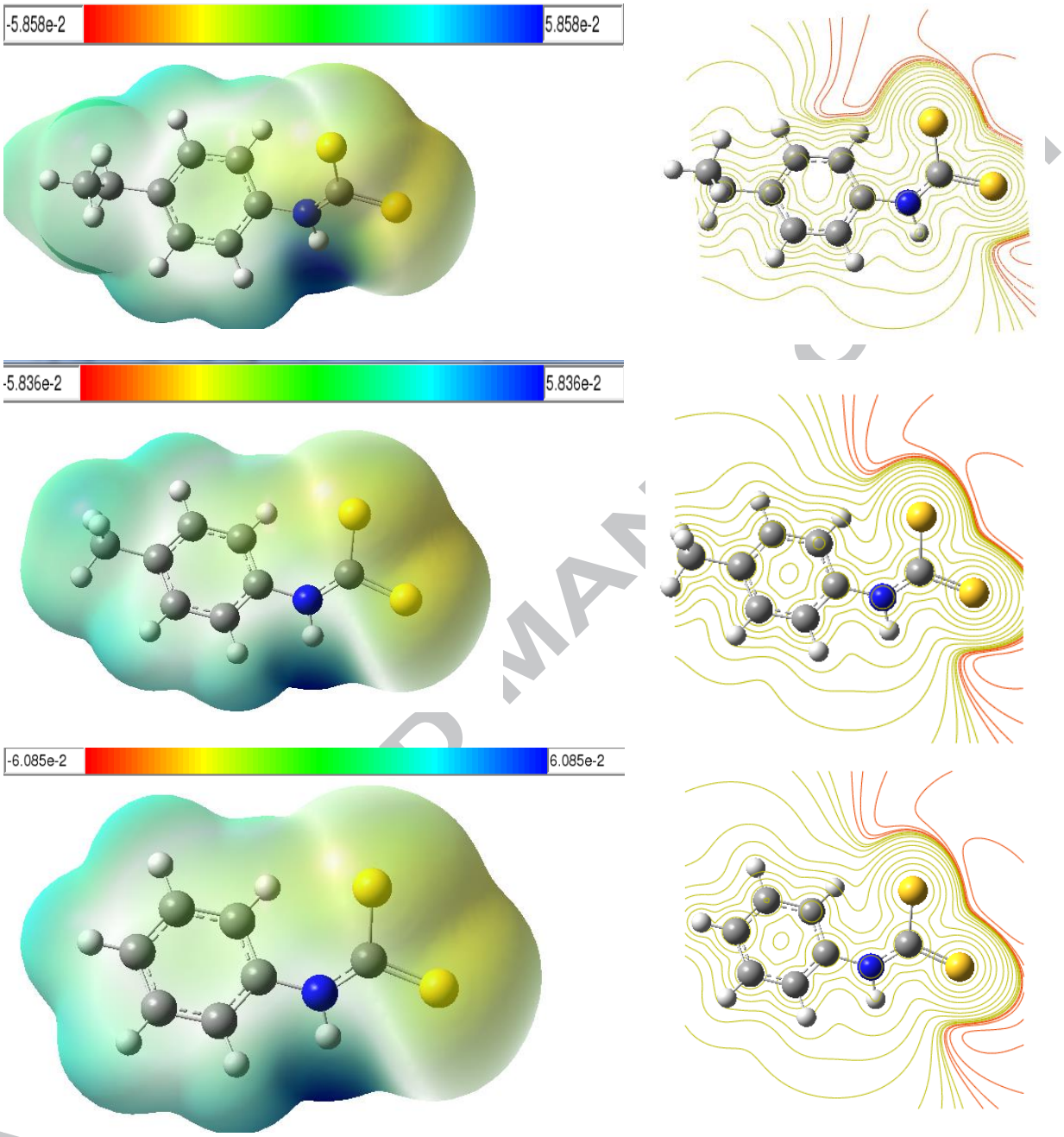

Fig. 5: Electrostatic potential maps and contour diagrams for the dithiocarbamate ligands. Contour value = 0.004 au.

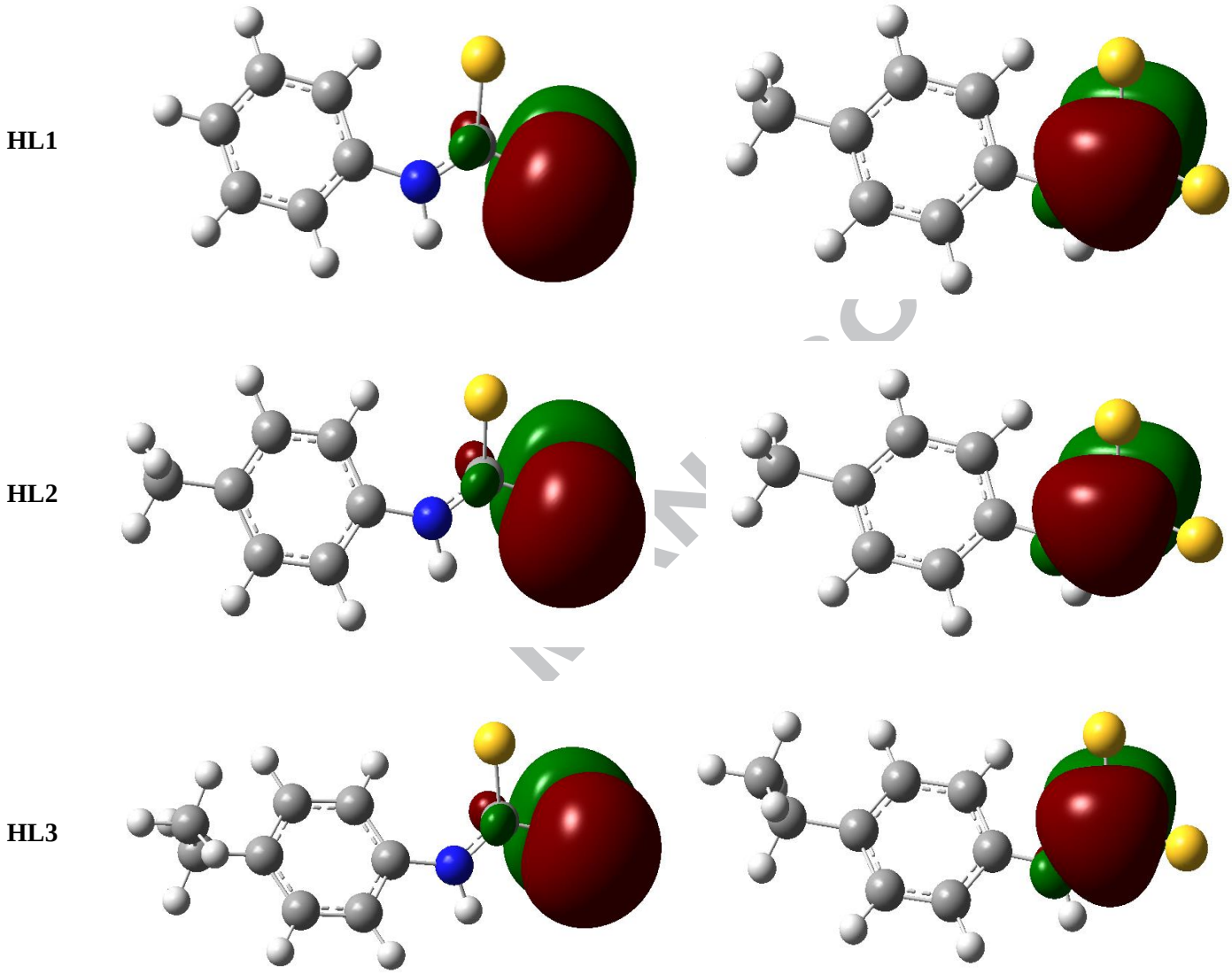

Fig. 6: Frontier molecular orbital diagrams for the 3 dithiocarbamate ligands. M.O. contour value = 0.02 au

	HOMO	LUMO
[Pt(L^1)2]	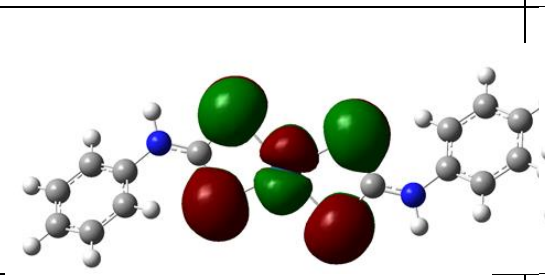	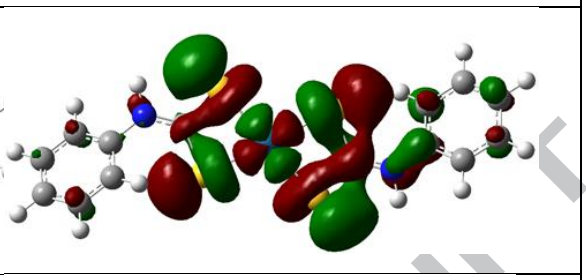
[Pt(L^2)2]	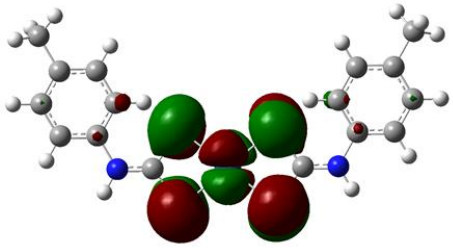	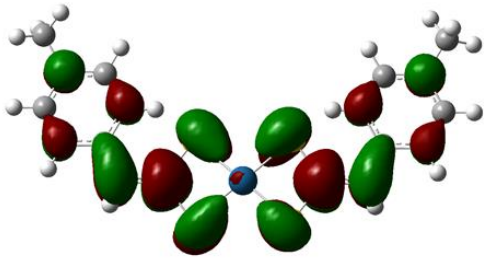
[Pt(L^3)2]	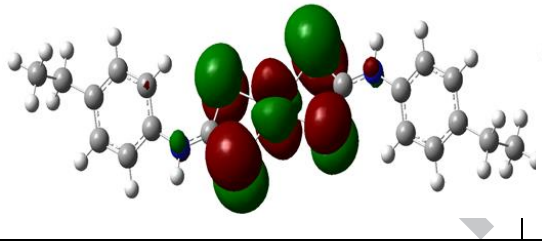	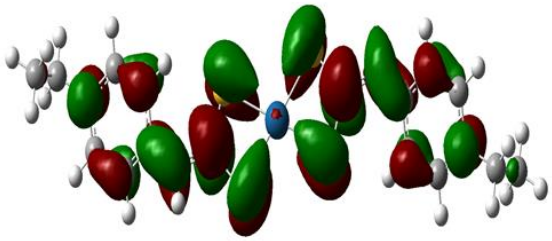
[Pd(L^1)2]	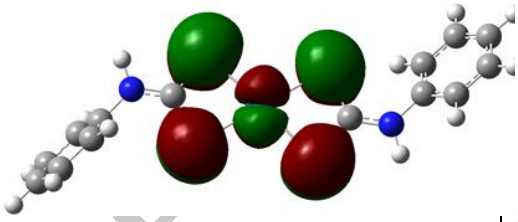	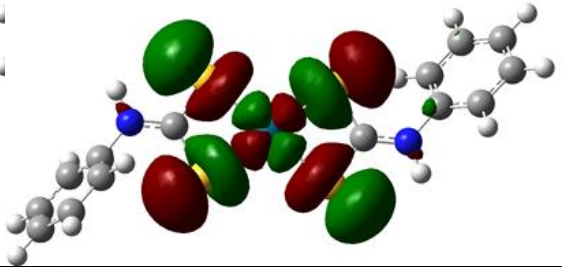
[Pd(L^2)2]	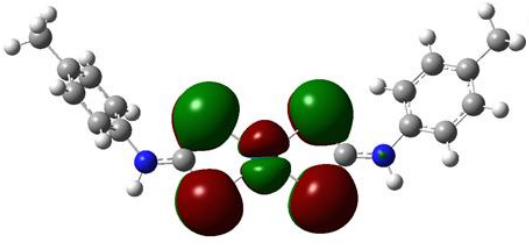	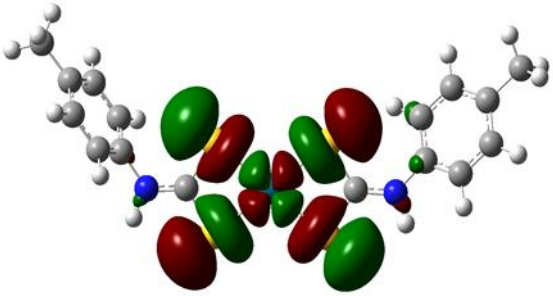
[Pd(L^3)2]	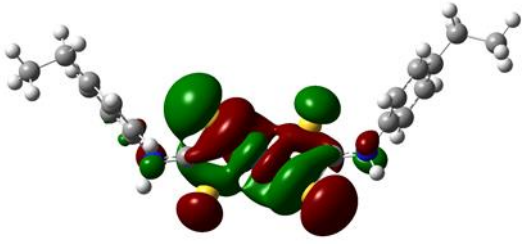	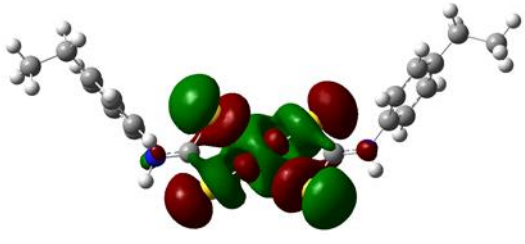

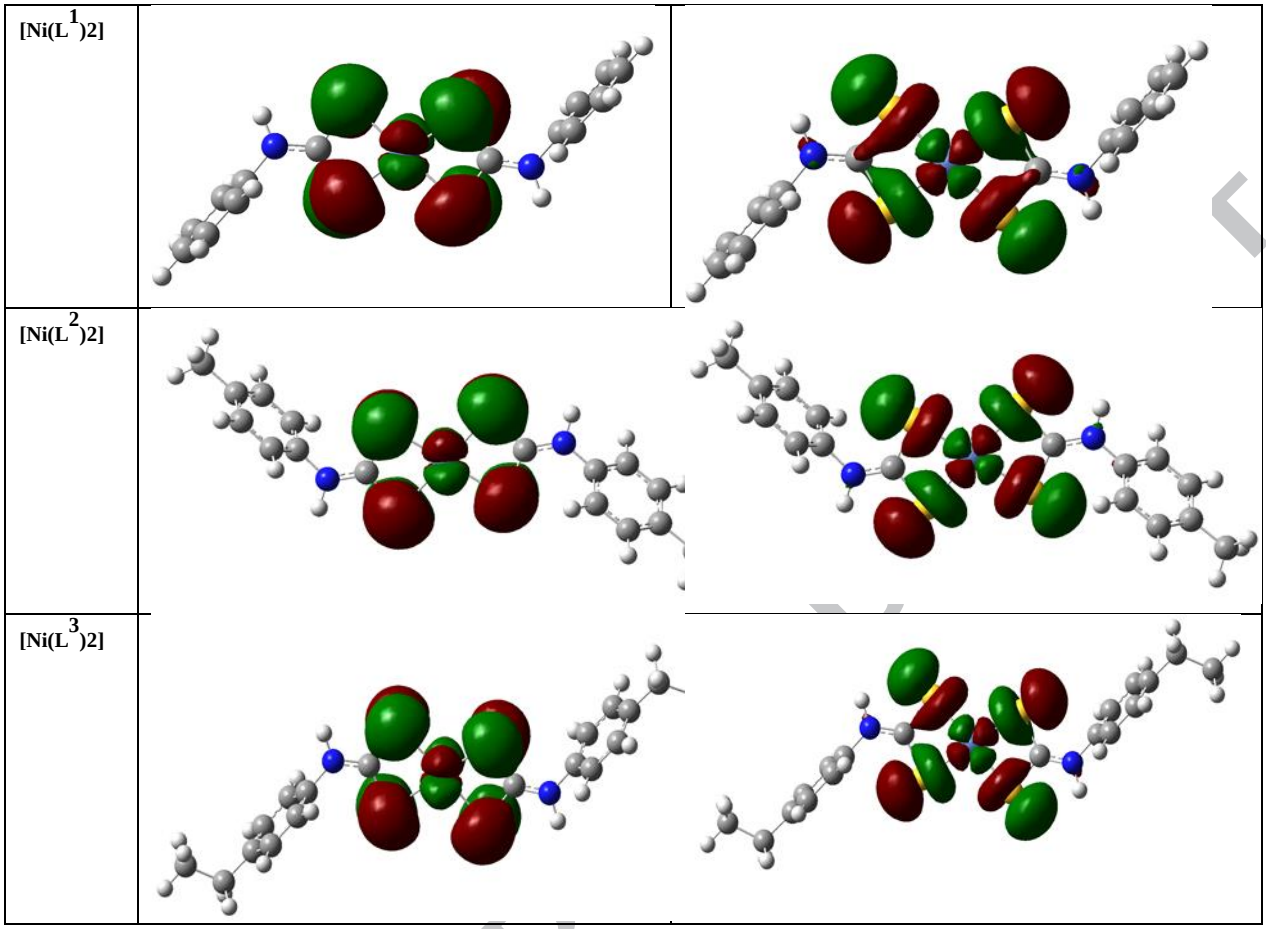

Fig. 7: Frontier molecular orbital diagrams for the platinum, palladium and nickel complexes of the dithiocarbamate ligands. M.O. contour value = 0.02 au

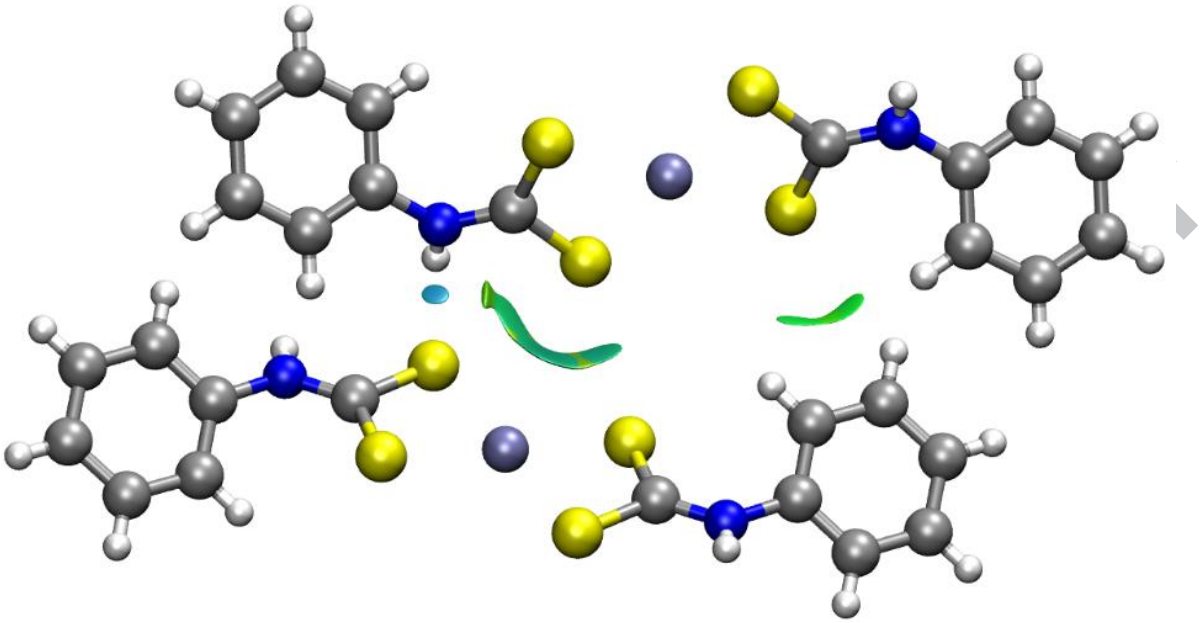

Fig. 8: 3-D isosurface plots of relevant non-covalent interactions in the palladium dithiocarbamate complex. Isovalue = 0.03 au

Table 1. Summary of crystal data and structure refinement for $[Pd(L^1)_2]$, $[Pt(L^1)_2]$ and $[Pt(L^3)_2]$

Complex	**$[Pd(L^1)_2]$**	**$[Pt(L^1)_2]$**	**$[Pt(L^3)_2]$**
Empirical formula	$C_{14}H_{12}N_2PdS_4$	$C_{14}H_{12}N_2PtS_4$	$C_{18}H_{20}N_2PtS_4$
Formula weight	442.90	531.59	587.6
Crystal size (mm)	0.29 × 0.23 × 0.07	0.28 × 0.13 × 0.09	0.47 × 0.37 × 0.26
Crystal system	orthorhombic	orthorhombic	Monoclinic
Temperature (K)	100	99.98	100
Crystal habit	Block, orange	Plate, yellow	Block, yellow
Space group	*Pbca* (no. 61)	*Pbca* (no. 61)	*P*21/*n* (no. 14)
a (Å)	9.5470(8)	9.6947(9)	10.9519(8)
b (Å)	6.5224(6)	6.4818(6)	8.2161(6)
c (Å)	24.393(2)	24.299(2)	11.7276(9)
α (°)	90	90	90
β (˚)	95.021(2)	96.111(2)	114.009(2)
α (°)	90	90	90
V [$Å^3$]	1518.9(2)	1527.0(2)	963.97(12)
Z	4	4	2
Dcalc (g cm^{-3})	1.937	2.312	2.025
F(000) Dataset	880 -12:12, -8:8, -32:32	1008 12:12, -8:8, -32:32	568 -14:14; -10:8; 15:15
μ(MoKa) (mm^{-1})	1.763	9.728	7.720
Tot.,Uniq.Data, R(int)	30730, 4612, 0.0645	21080, 2295, 0.024	72891, 2086, 0.027
Observed reflections $I > 2\sigma(I)$	1630	1476	2157
V [Å**3]	1518.9(2)	1527.0(2)	963.97(12)
Nref, Npar	4612, 209	2295, 110	2427, 119
Final R, wR2, S	0.0233, 0.0587 , 1.09	0.0198, 0.0384, 1.03	0.018, 0.043, 1.09
Max. residual density [e $Å^{-3}$]	-0.35, 0.49	-0.64, 0.49	-0.41, 1.26
Min. residual density [e $Å^{-3}$]	2.7–28.3	2.7-28.3	3.1–28.4

Table 2. Selected bond distances and angles for $[Pd(L^1)_2]$, $[Pt(L^1)_2]$ and $[Pt(L^3)_2]$

$[Pd(L^1)_2]$		**$[Pt(L^1)_2]$**		**$[Pt(L^3)_2]$**	
Bond	Distance (Å)	Bond	Distance (Å)	Bonds	Distances (Å)
Pd1—S1	2.3232(5)	Pt1—S1	2.3201(7)	Pt1-S1	2.3163(6)
Pd1—S1i	2.3232(5)	Pt1—S1 i	2.3202(7)	Pt1—S1i	2.3163(6)
Pd1—S2i	2.3399(5)	Pt1—S2	2.3313(7)	Pt1– S2	2.3216(6)
Pd1—S2	2.3399(5)	Pt1—S2 i	2.3314(7)	Pt1—S2i	2.3216(6)
S1-C1	1.724(2)	S1—C1	1.731(3)	S1– C1	1.726(3)
S2-C1	1.707(2)	S2—C1	1.704(3)	S2– C1	1.716(2)
N1—C1	1.324(2)	N1—C1	1.327(4)	N1-C1	1.327(3)
N1—C2	1.420(2)	N1—C2	1.426(4)	N1-C2	1.423(3)
C2—C3	1.390(3)	C2—C3	1.389(4)	N1—H1	0.80(3)
Bond	Angle (˚)	Bond	Angle (˚)	Bond	Angle (˚)
S1—Pd1—S1i	180.0	S1—Pt1—S1i	180.0	S1 – Pt1 – S11	180
S1—Pd1—S2i	75.134(17)	S1—Pt1—S2	74.75(3)	S1– Pt1 – S21	105.07(2)
S1—Pd1—S2	104.866(17)	S1—Pt1—S2	105.24(3)	S1—Pt1—S2	74.93(2)
S1—Pd1—S2i	104.864(17)	S1—Pt1—S2i	105.25(3)	S1—Pt1—S2i	74.93(2)
S1—Pd1—S2	75.136(17)	S1—Pt1—S2i	74.76(3)	S1—Pt1—S2i	105.07(2)
S2—Pd1—S2	180.00(2)	S2—Pt1—S2	180.00(19)	S2—Pt1—S2	180.0
C1—S1—Pd1	86.17(7)	C1—S1—Pt1	86.95(10)	Pt1–S1 –C1	87.40(8)
C1—S2—Pd1	86.03(7)	C1—S2—Pt1	87.20(10)	Pt1–S2– C1	87.47(9)
C1—N1—H1	112.5(17)	C1—N1—H1	117(2)	C1—N1—H1	117(2)
C1—N1—C2	129.33(18)	C1—N1—C2	129.1(3)	C1—N1—C2	130.4(2)
C2—N1—H1	117.9(17)	C2—N1—H1	113(2)	C2—N1—H1	113(2)
S2—C1—S1	111.92(11)	S2—C1—S1	110.61(16)	S2—C1—S1	110.08(14)
N1—C1—S1	120.46(16)	N1—C1—S1	120.5(2)	N1—C1—S1	127.61(19)
N1—C1—S2	27.58(16)	N1—C1—S2	128.9(2)	N1—C1—S2	122.30(19)
C3—C2—N1	117.43(19)	C3—C2—N1	117.5(3)	C3—C2—N1	123.6(2)

Table 3. Hydrogen-bond geometry (Å, º) for $[Pt(L^1)_2]$

D—H···*A*	*D*—H	H···*A*	*D*···*A*	*D*—H···*A*
N1—H1···S1^{ii}	0.80(4)	2.62(4)	3.407(3)	169(3)

Symmetry code: (ii) -*x*+3/2, *y*+1/2, *z*.

Table 4. Hydrogen-bond geometry (Å, º) for [Pd(L^1)$_2$]

D—H···*A*	*D*—H	H···*A*	*D*···*A*	*D*—H···*A*
N1—H1···S1^{ii}	0.80(2)	2.61(2)	3.4104(19)	175(2)

Symmetry code: (ii) -*x*+3/2, *y*+1/2, *z*.

Table 5. Hydrogen-bond geometry (Å, º) for [Pt(L^2)$_2$]

D—H···*A*	*D*—H	H···*A*	*D*···*A*	*D*—H···*A*
N1—H1···S1^{ii}	0.80(3)	2.90(3)	3.659(2)	159(3)

Symmetry code: (ii) -*x*+3/2, *y*-1/2, -*z*+1/2.

Table 6. Thermal stability data for the metal complexes

COMPOUND	DECOMPOSITION RANGE (◦C)	PEAK TEMP (◦C)	WEIGHT LOSS (%)	PRODUCT OBTAINED	MASS CHANGE (mg)
[Ni(L^1)$_2$]	163 - 215	192	75	NiS	2.78/2.60

$[Pd(L^1)_2]$	269 - 290	232	68	PdS	3.84/4.10
$[Pt(L^1)_2]$	199 - 300	250	54	PtS_2	5.65/5.57
$[Ni(L^2)_2]$	174 - 209	187	78	NiS	2.39/2.23
$[Pd(L^2)_2]$	171 - 305	234	67	PdS	3.40/3.24
$[Pt(L^2)_2]$	213 - 380	252	60	PtS	4.95/4.59
$[Ni(L^3)_2]$	138 - 450	191	66	PtS	4.40/4.70
$[Pd(L^3)_2]$	144 - 274	200	75	PdS	3.30/3.60
$[Pt(L^3)_2]$	138 - 450	191	66	PtS	4.40/4.70

Table 7: Summary of the antimicrobial screening results of the metal complexes

S/N	Compound	*S. aureus*	*K.Pneumonia*	*B. Cereus*	*E.Coli*	*P.Aeruginosa*	*C. Albican*	*A. flavus*
1	$[Ni(L^1)_2]$	-	11 ±0.4	-	10 ±0.4	11 ±0.7	-	-
2	$[Pd(L^1)_2]$	10 ±0.0	-	08 ±1.4	17 ±0.0	11 ±0.0	13 ±0.0	-
3	$[Pt(L^1)_2]$	08 ± 1.4	16 ±1.4	-	11 ±0.7	14 ±0.0	07 ±1.4	-
4	$[Ni(L^2)_2]$	14 ±0.7	11 ±0.7	-	12 ±0.7	-	-	-
5	$[Pd(L^2)_2]$	-	13 ±0.0	-	15 ±0.7	11 ±0.0	11 ±1.4	-
6	$[Pt(L^2)_2]$	-	11 ±1.4	09 ±1.4	10 ±1.4	11 ±0.7	07 ±1.4	14 ±0.7
7	$[Ni(L^3)_2]$	18 ±1.2	17 ±0.7	20 ±0.7	18 ±04	15 ±0.7	12 ±0.7	-
8	$[Pd(L^3)_2]$	19 ±0.7	19 ±0.7	21 ±0.7	16 ±0.7	14 ±0.0	08 ±1.4	10 ±0.7
9	$[Pt(L^3)_2]$	26 ±0.0	20 ±0.7	23 ±0.7	20 ±0.4	23 ±0.7	15 ±0.4	12 ±1.4
10	Sulfamethoxazole	23 ±0.7	26 ±0.0	26 ±0.4	30 ± 0.4	28 ±0.0	-	-
11	Ketoconazole	-	-	-	-	-	27 ±0.7	22 ±0.7

Table 8: HOMO and LUMO energy gap and reactivity parameters at different levels of theory for the 3 ligands

Parameters	L^1			L^2			L^3		
	B3LYP	M062x	ωB97XD	B3LYP	M062x	ωB97XD	B3LYP	M062x	ωB97XD
E_{HOMO} (eV)	-6.635	7.851	-8.866	-6.556	-7.776	-8.580	-6.556	-7.778	-8.509
E_{LUMO} (eV)	-1.792	0.751	0.2889	-1.692	-0.623	-0.129	-1.692	-0.635	-0.363
$\Delta E_{HOMO-} E_{LUMO}$ (ev)	4.868	7.100	8.866	4.864	7.153	8.451	4.468	7.142	8.872
Electronegativity (χ)	4.213	4.301	4.144	4.124	4.196	4.356	4.123	4.207	4.073
Chemical hardness (η)	2.422	3.556	4.433	2.432	3.576	4.266	2.434	3.572	4.436
Global softness (σ)	0.413	0.282	0.226	0.411	0.279	0.236	0.411	0.280	0.225
Electrophilicity index (ω)	3.664	2.605	1.963	3.496	2.455	2.245	3.486	2.477	1.869
Chemical potential (μ)	-4.213	-4.301	-4.144	-4.124	-4.196	-4.356	-4.123	-4.207	-4.073

Table 9: HOMO-LUMO energies and global reactivity parameters for the Pt, Pd and Ni complexes of the dithiocabarmate ligands

Complex	E_{HOMO} (ev)	E_{LUMO} (ev)	ΔE_{L-H} (ev)	η (ev)	σ (ev)	ω(ev)	Dipole moment (Debye)
$[NiL^1)2]$	-5.823	-2.180	3.643	1.821	0.549	4.397	8.985
$[NiL^2)2]$	-5.739	-2.097	3.642	1.820	0.549	4.251	9.149
$[NiL^3)2]$	-5.742	-2.101	3.641	1.821	0.549	4.223	8.766
$[PdL^1)2]$	-5.809	-2.309	3.501	1.751	0.571	4.702	9.177
$[PdL^2)2]$	-5.725	-2.226	3.499	1.749	0.571	4.516	9.364
$[PdL^3)2]$	-5.726	-2.226	3.500	1.750	0.560	4.516	8.977
$[PtL^1)2]$	-5.468	-1.733	3.735	1.868	0.535	3.471	8.835
$[PtL^2)2]$	-5.386	-1.650	3.736	1.867	0.535	3.312	9.084
$[PtL^3)2]$	-5.422	-1.627	3.794	1.897	0.527	3.273	8.860

Graphical Abstract

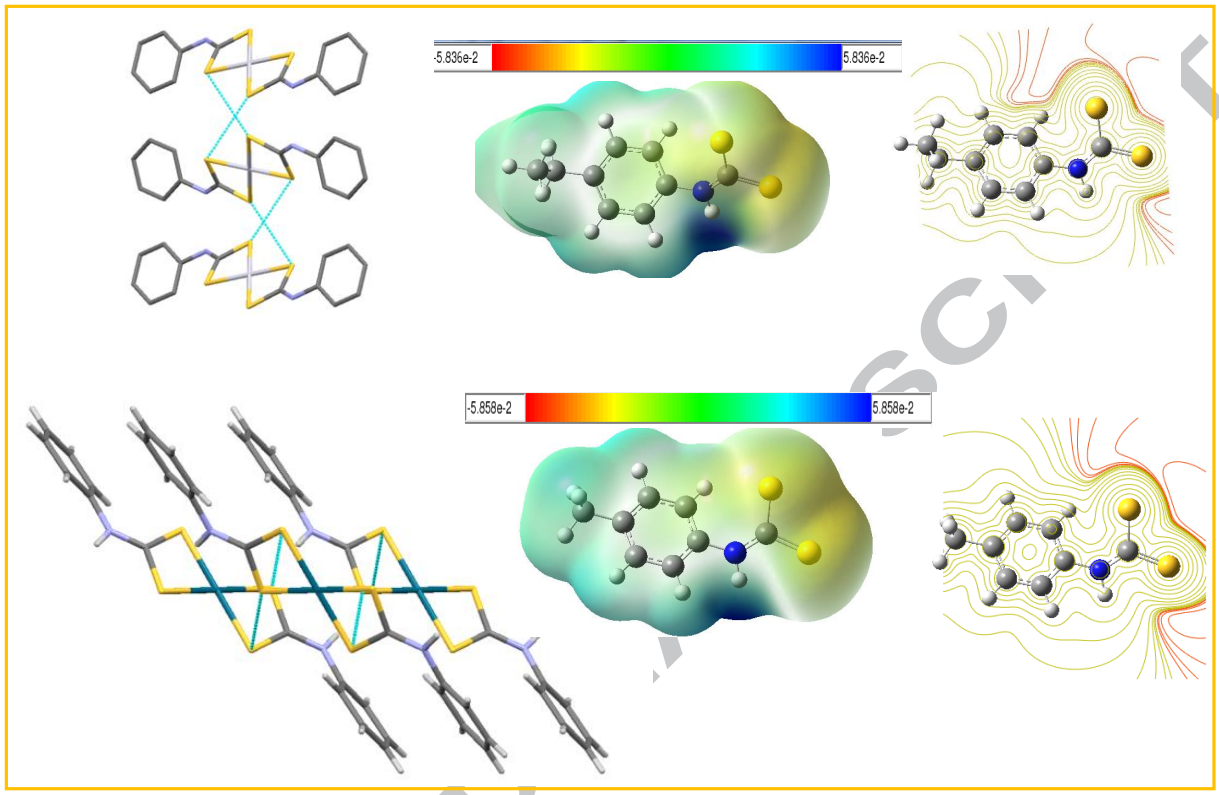

GA synopsis

Group 10 metal complexes of dithiocarbamates derived from primary amines were prepared and DFT was used to study their electrostatic potential maps, frontier molecular orbitals and contours of the ligands. The frontier molecular orbitals for the platinum, palladium and nickel complexes, as well as their antimicrobial potency, were also reported.